Jon Blundy · Kathy Cashman

Ascent-driven crystallisation of dacite magmas at Mount St Helens, 1980–1986

Received: 30 July 1999 / Accepted: 10 August 2000 / Published online: 11 January 2001 © Springer-Verlag 2001

Abstract We introduce a novel scheme that enables natural silicic glasses to be projected into the synthetic system Qz-Ab-Or-H₂O in order to relate variations in volcanic glass chemistry to changing pressure (P) and temperature (T) conditions in the sub-volcanic magma system. By this means an important distinction can be made between ascent-driven and cooling-driven crystallisation under water-saturated or undersaturated conditions. In samples containing feldspar and a silica phase (quartz or tridymite), quantitative P–T estimates of the conditions of last equilibrium between crystals and melt can be made. Formation of highly silicic melts (i.e. > 77 wt% SiO₂) is a simple consequence of the contraction of the silica phase volume with decreasing pressure, such that high silica glasses can only form by crystallisation at low pressure. Resorption of quartz crystals appears to be a further diagnostic feature of decompression crystallisation. Groundmass and inclusion glasses in dacites from the 1980-1986 eruption of Mount St Helens volcano (WA) span a wide range in SiO₂ (68–80 wt%, anhydrous). The compositions of the least evolved (SiO₂-poor) inclusions in amphibole phenocrysts record entrapment of silicic liquids with ≤ 5.4 wt% water, corresponding to a water saturation pressure of ~200 MPa at 900 °C. The compositions of more evolved (higher SiO₂) plagioclase-hosted inclusions and groundmass glasses are consistent with extensive ascent-driven fractional crystallisation of plagioclase, oxide and orthopyroxene phenocrysts and microlites to low pressures. During this polybaric crystallisation, plagioclase phenocrysts trapped melts with a wide range of dissolved water contents (3.5–5.7 wt%). Magmas

glass chemistry and groundmass texture two arrest levels have been identified, at depths of 0.5-1 and 2-4 km. A single dome sample from February 1983 contains groundmass plagioclase, tridymite and quartz, testifying to temperatures of at least 885 °C at 11 MPa. These shallow storage conditions are comparable to those in the cryptodome formed during spring 1980. The corresponding thermal gradient, ≤ 0.2 °C MPa⁻¹, is consistent with near-adiabatic magma ascent from ~8 km. We argue that the crystallisation history of Mount St Helens dacite magma was largely a consequence of decompression crystallisation of hot magma beyond the point of water saturation. This challenges the conventional view that phenocryst crystallisation occurred by cooling in a large magma chamber prior to the 1980–1986 eruption. Because the crystallisation process is both polybaric and fractional, it cannot be simulated directly using isobaric equilibrium crystallisation experiments. However, calculation of the phase proportions in watersaturated 910 ± 15 °C experiments by Rutherford et al. (1985) over the pressure range 220–125 MPa reproduces the crystallisation sequence and phenocryst modes of Mount St Helens dacites from 18 May 1980. By allowing for the effects of fractional versus equilibrium crystallisation, entrained residual source material, and small temperature differences between nature and experiment, phase compositions can also be matched to the natural samples. We conclude that decompression of watersaturated magma may be the dominant driving force for crystallisation at many other silicic volcanic centres.

erupted during the Plinian phase of the 18 May 1980

eruption were derived from a large reservoir at depths of

≥6 km. Subsequent magmas ascended to varying depths

within the sub-volcanic system prior to extraction. From

J. Blundy (🖂) CETSEI, Department of Earth Sciences, University of Bristol, Bristol BS8 1RJ, UK e-mail: jon.blundy@bristol.ac.uk

K. CashmanDepartment of Geological Sciences,University of Oregon, Eugene, OR 97403-1272, USAEditorial responsibility: I. S. E. Carmichael

Introduction

Quartz-saturated rhyolites and granites are derived from melts that contain, at most, \sim 77.4 wt% SiO₂ (Hildreth 1981), consistent with pre-eruptive magma storage at

depths of $\sim 7-8$ km (pressures of ~ 200 MPa). During eruption these melts moved rapidly from storage to the surface with negligible subsequent crystallisation. In contrast, more highly evolved glasses (≤79-80 wt% SiO₂) are common in volcanic pyroclasts and lavas of intermediate composition that have experienced extensive, low pressure crystallisation during magma ascent (e.g. Melson 1983; Cashman 1992; Geschwind and Rutherford 1995; Wolf and Eichelberger 1997; Hammer et al. 1999). Here, we show that experiments on natural and synthetic systems can shed light on the process of decompression-induced crystallisation. In particular, we show that the evolution of melt to extremely SiO₂-rich compositions requires crystallisation at very low pressures, and that extensive co-precipitation of quartz and feldspar only occurs when magma ascent is accompanied by significant cooling. We illustrate these hypothetical P-T paths using new and previously published groundmass glass compositions from the 1980-1986 eruption of Mount St Helens. We then compare groundmass glass compositions with those of phenocryst-hosted melt inclusions to propose a new, polybaric fractionation model for Mount St Helens 1980-1986 magmas.

Experimental phase relations in synthetic silicic systems

Low-pressure (< 100 MPa) phase relations are poorly defined for natural and synthetic silicic systems because kinetic barriers can prevent viscous melts from attaining equilibrium on experimental time-scales (e.g. Schairer 1950). However, phase relations in the 'haplogranite' system quartz-albite-orthoclase are well constrained for water-saturated conditions at pressures between 50 and 500 MPa (Tuttle and Bowen 1958), and for water-undersaturated conditions at 200 and 500 MPa (Holtz et al. 1992a). Additionally, a number of studies have extended the haplogranite system to include anorthite (An; James and Hamilton 1969; Winkler and Ghose 1973; Winkler et al. 1975, 1997), and corundum (Cor; Holtz et al. 1992b). An excellent synthesis of the available information can be found in Johannes and Holtz (1996). Here, we summarise the main findings of these experiments, and illustrate chemical variation in watersaturated and water-undersaturated haplogranitic melts crystallised under a variety of conditions.

At pressures below 500 MPa, the Qz–Ab–Or–H₂O system is characterised by two primary phase volumes (quartz and feldspar) separated by a curved cotectic (Fig. 1). Because of complete solid solution between albite and orthoclase on the solidus at low pressure (Bowen and Tuttle 1950), the cotectic contains a minimum rather than a eutectic. The location of the cotectic, and its minimum, shift systematically with water pressure. For water-saturated conditions, the silica phase volume decreases (i.e. silica solubility increases) with decreasing pressure, whereas the minimum moves towards the Qz–Or join. At pressures of ≥500 MPa,

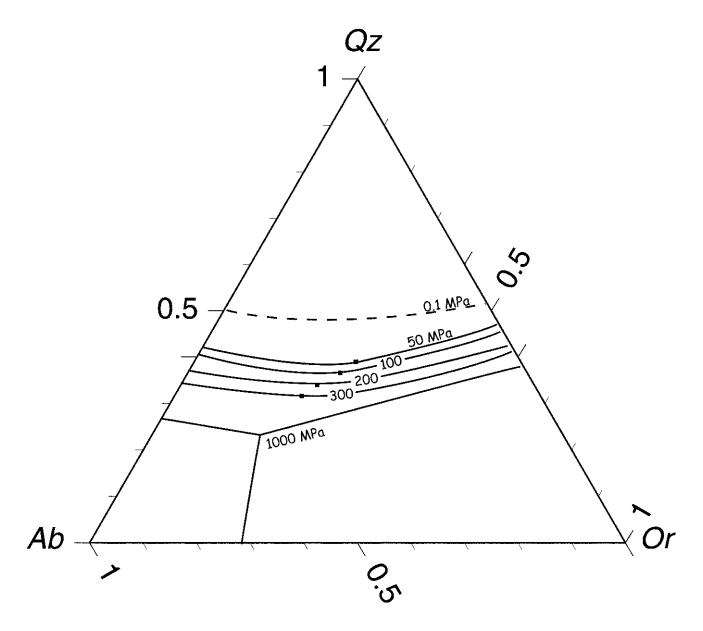


Fig. 1 Cotectic lines and compositions of H₂O-saturated minima and eutectics in Qz–Ab–Or haplogranitic melts as a function of pressure (500 MPa curve omitted for clarity). Units are weight fraction. Data from Tuttle and Bowen (1958), Luth et al. (1964), Ebadi and Johannes (1991)

there is a miscibility gap between K- and Na-feldspar and the ternary minimum becomes a eutectic connected to the Ab–Or binary by a two-feldspar cotectic. With decreasing pressure the temperature of the minimum (or eutectic) increases sharply, from 645 °C at 500 MPa, to 680 °C at 200 MPa, to ~950 °C at atmospheric pressure (Tuttle and Bowen 1958). Water undersaturation has relatively little effect on the position of the cotectic at any given pressure, but shifts the minimum towards the Qz–Or join, and increases its temperature. For example, at 200 MPa the minimum temperature changes from 764 °C at a water activity ($a_{\rm H_2O}$) of 0.5 to 902 °C at $a_{\rm H_2O}$ =0.1. Water solubility at the composition of the minimum increases with increasing pressure, from ~2.2 wt% at 50 MPa, to nearly 10 wt% at 500 MPa.

The stable liquidus silica phase is high quartz, except at pressures below ~20 MPa, where tridymite appears near the ternary minimum. At still lower pressures tridymite becomes the stable silica phase along the entire cotectic (Tuttle and Bowen 1958). There are no reliable experimental data on the Qz–Ab–Or ternary at pressures below 50 MPa because of difficulties in attaining equilibrium on experimental time scales. However, the location of the silica–feldspar cotectic, which represents the maximum possible Qz-content of an An-free haplogranitic feldspar-saturated liquid can be estimated from the experiments of Schairer (1950).

Using the experimental data described above, it is possible to determine fractionation paths for any water-saturated or water-undersaturated haplogranite composition under a variety of crystallisation conditions. Here we discuss three cases of relevance to the crystallisation of natural silicic magmas:

- 1. isobaric (200 MPa) cooling from 800 °C, under water-saturated conditions (Fig. 2a);
- 2. isothermal (800 °C) decompression from 200 MPa, under water-saturated conditions (Fig. 2b);
- 3. isothermal (890 °C) decompression from 200 MPa, with a fixed initial water content of 4 wt% (Fig. 2c).

Our choice of conditions is designed to reflect idealised scenarios for shallow sub-volcanic magmas. Our choice of starting composition, Qz₁₆Ab₇₅Or₉, is similar to the CIPW normative composition of many natural dacites (see below). Each fractionation path is calculated using the data of Tuttle and Bowen (1958) and/or Johannes and Holtz (1996) for pressures of 50–200 MPa. At pressures below 50 MPa, we are informed by the partially schematic phase diagrams of Tuttle and Bowen (their Fig. 33), data on the Ab–Qz binary (their Fig. 27), and the phase diagram of silica (their Fig. 12). In our calculations we assume perfect fractional crystallisation. In reality, crystals will not efficiently segregate from viscous silicic melts, and although feldspars are commonly zoned, minor retention of quartz will render fractionation somewhat imperfect.

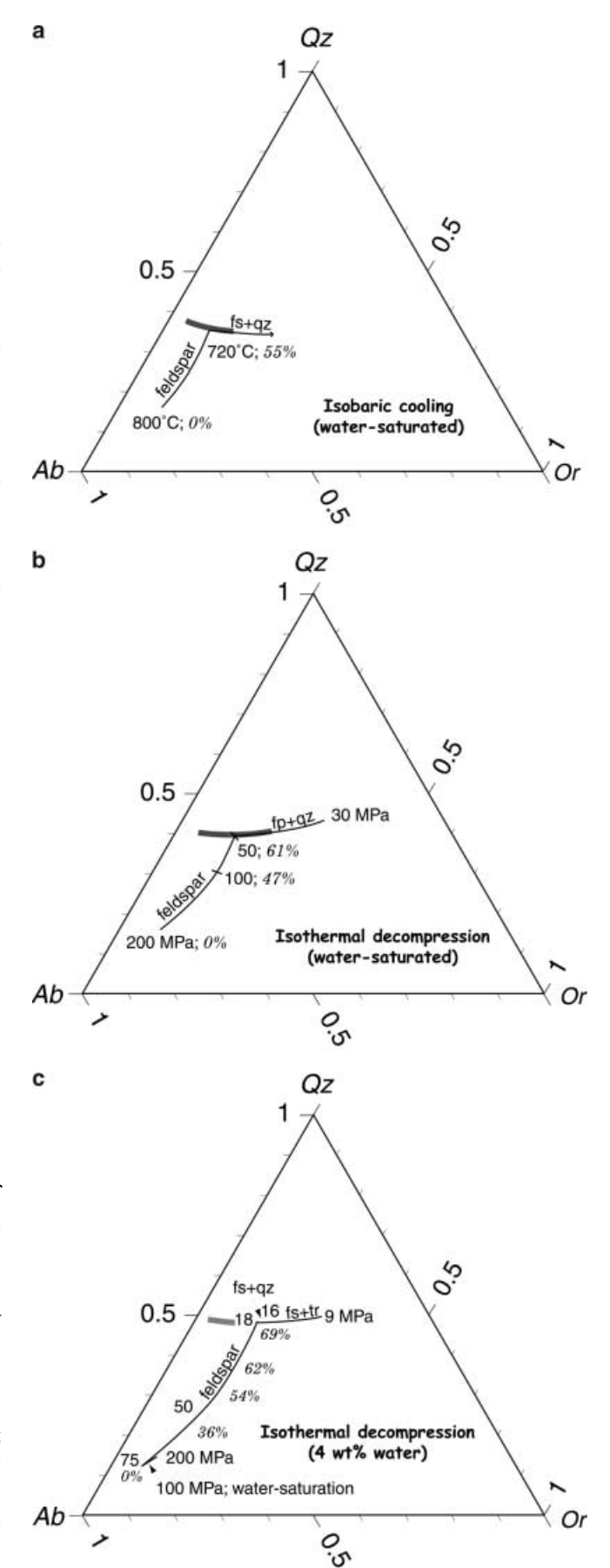
Water-saturated isobaric cooling (Fig. 2a)

The fractionation path at 200 MPa, from an initial temperature of 800 °C, is similar to that at 100 MPa shown in Tuttle and Bowen (1958; their Fig. 30). The melt follows a curved trajectory, crystallising increasingly potassic feldspar, until it reaches quartz saturation at 720 °C. At this point the original crystal-free melt is 55% crystallised. With subsequent cotectic precipitation of high quartz and increasingly potassic feldspar, the melt reaches the ternary minimum at 680 °C, where crystallisation proceeds to completion. Cotectic crystallisation is marked by near-constant Qz content of the melt. The maximum Qz content attained is 36%.

Water-saturated isothermal decompression (Fig. 2b)

The isothermal fractionation path at 800 °C, with a starting pressure of 200 MPa, is also similar to that of Tuttle and Bowen (1958; their Fig. 32), calculated at 760 °C and a starting pressure of 300 MPa. As in the

Fig. 2 Calculated crystallisation paths in the haplogranitic system for an initial composition $Qz_{16}Ab_{75}Or_{9}$. Crystallising phases labelled as feldspar (fs), tridymite (tr) and quartz (qz). Percentage crystallisation at selected points along the curves is given in *italics*. The *heavy black line* shows the evolution of qz + fs extracts during cotectic crystallisation. a Water-saturated isobaric cooling at 200 MPa, of melt with 0% initial crystals. b Water-saturated isothermal decompression at 800 °C of melt with 0% initial crystals. c Water-undersaturated isothermal decompression at 890 °C of melt with 4 wt% dissolved H_2O and 10% initial feldspar crystals. Calculated from data of Tuttle and Bowen (1958), Holtz et al. (1992a)



case of isobaric cooling, the originally crystal-free melt follows a curved fractionation path and crystallises increasingly potassic feldspar. The melt attains quartz saturation at 50 MPa, at which point it is about 61% crystallised. High quartz and increasingly potassic feldspar then crystallise along the cotectic. Because of the shift in the ternary minimum with pressure, the isothermal, polybaric cotectic is oblique to its isobaric counterpart, such that, along the polybaric cotectic, the Qz content of the melt increases slightly and the quartz:feldspar ratio of the crystalline residue decreases. Crystallisation is completed at ~30 MPa, i.e. the pressure at which the temperature of the water-saturated haplogranite minimum is 800 °C. The maximum Qz content attained in the melt is 43%.

An interesting corollary of the migration of the cotectic towards Qz with decreasing pressure is that a melt in equilibrium with quartz and feldspar at high pressure will lie outside the quartz phase volume at lower pressure. Consequently, if decompression occurs suddenly then any retained quartz crystals formed at higher pressure may be resorbed at the same time as feldspar is crystallising (Whitney 1988).

Water-undersaturated isothermal decompression (Fig. 2c)

This case, which was not discussed by Tuttle and Bowen (1958), is constructed from their data at water-saturated conditions (≤ 200 MPa), and those of Holtz et al. (1992a) for 200-MPa water-undersaturated conditions. With 4 wt% H_2O at 200 MPa, a_{H_2O} is ~ 0.55 , and the liquidus temperature for Qz₁₆Ab₇₅Or₉ is 890 °C. As the magma ascends, the liquidus temperature will decrease at a rate of ~0.5°C/MPa (Johannes and Holtz 1996; their Fig. 2.26). This is an important feature of water-undersaturated magmas, and means that any feldspar crystals initially present in the magma will become resorbed during the initial stages of isothermal ascent as $a_{\rm H2O}$ increases to 1.0. In an attempt to illustrate this phenomenon we consider that at 200 MPa the magma contains 10% suspended feldspar crystals. These might, for example, be phenocrysts formed on the liquidus at greater depth, entrained residual source material, or accidental xenocrysts. As this magma ascends, the melt will resorb the feldspar and the melt composition will track the 890 °C isotherm towards Ab. Feldspar will be totally resorbed by ~ 160 MPa, when the magma will be fully molten. At 100 MPa, the melt, which now has slightly less than 4 wt% H₂O because of feldspar resorption, will attain water saturation and H₂O vapour bubbles will form. The melt finally intersects the water-saturated liquidus at \sim 75 MPa, and crystallisation can begin. (If more crystals were present initially, the melt would migrate further towards Ab, and water-saturated crystallisation would begin at slightly higher pressures.) Overall, the melt composition changes relatively little during this water-undersaturated phase of ascent (Fig. 2c).

Subsequent magma ascent is marked by continuous crystallisation along a curved path, very similar to that for the water-saturated case. However, because of the higher initial temperature, fractionation can proceed to much lower pressures before intersecting the solidus. At the point of quartz saturation (\sim 18 MPa) the initial melt is 69% crystallised. With further decompression, the melt encounters the high quartz-tridymite phase boundary at 16 MPa (the pressure at which 890 °C lies on the quartz-tridymite phase boundary; e.g. Johannes and Holtz 1996) and subsequent cotectic crystallisation involves tridymite + feldspar. There are insufficient experimental data to constrain accurately the shift in the position of the cotectic at pressures below 50 MPa. However, following Fig. 33 of Tuttle and Bowen (1958), we speculate that the cotectic shifts little over this pressure interval. For this reason we show the polybaric cotectic almost parallel to the isobaric case, and infer that there is very little Qz increase in the melt during cotectic crystallisation (i.e. the scope for quartz-resorption during imperfect fractional crystallisation is limited relative to higher pressures, e.g. case (2) discussed above). Crystallisation goes to completion at the ternary minimum at ~9 MPa. The maximum Qz content attained in the melt is 50%.

The three cases we have considered are overly simplistic. For example, isothermal ascent is unlikely (adiabatic or isentropic ascent is more probable; Johannes and Holtz 1996) and perfect fractional crystallisation is untenable in viscous silicic melts. Nonetheless, our three cases can be used to illustrate a number of important processes in sub-volcanic systems. First, highly silicic (Qz-rich) melts can only be produced by crystallisation at low pressure: the lower the final crystallisation pressure, the higher the Qz content. Such melts may saturate with quartz, or in extreme cases, tridymite, at low pressure. Because of their low crystallisation pressure, Qz-rich melts will be relatively water-poor.

Second, the depth at which silicic magma encounters its solidus depends on its temperature and water content (e.g. Fyfe 1970; Whitney 1988; Johannes and Holtz 1996): hot, relatively dry ($a_{\rm H2O}$ < 1) magma can continue to crystallise to very shallow depths, whereas cool, wet ($a_{\rm H_2O}$ = 1) magma encounters its solidus at a greater depth.

Third, ascent of water-undersaturated magma is characterised by feldspar resorption up to the point of water saturation. As a consequence, water-undersaturated silicic magmas crystallise over a much narrower depth interval than their water-saturated counterparts (Whitney 1988). Thus, in the examples in Fig. 2b, c, water-saturated magma undergoes 60% crystallisation over the pressure interval 200–50 MPa (~6 km), whereas for initially water-undersaturated magma the same extent of crystallisation takes place between 85 and 30 MPa (~2 km).

Finally, during ascent-driven crystallisation quartz may be resorbed at the same time as feldspar is crystallising if ascent is too rapid to allow the melt composition to track the migration of the cotectic towards Qz. This will not occur during crystallisation driven by isobaric cooling. A special case is that of ascent-driven crystallisation of relatively hot water-undersaturated magma in which resorbed quartz crystals may occur in association with later-precipitated tridymite. We note also that if quartz nucleation is kinetically impeded in highly viscous silicic melt then some overstepping of the cotectic (supersaturation) may occur.

Application to natural silicic magmas

The conclusions derived from the Qz-Ab-Or ternary can, in principle, be extended to natural silicic melts with elevated normative Oz, Ab and Or. However, to apply these results we must account for the effect of components not present in haplogranites, such as Ca, Fe and Mg. Cursory inspection of the Qz–Ab–An ternary shows that anorthite, a ubiquitous normative component in natural silicic rocks, substantially displaces the position of the quartz-feldspar cotectic to higher Qz contents (Yoder 1968; Johannes and Holtz 1996). Similarly, in the feldspar ternary (Ab-Or-An), the addition of a few percent An first creates a two-feldspar cotectic and then displaces it to higher Or contents (Brown 1993). Unless such effects are considered, it is not possible to make quantitative deductions about the ascent and crystallisation of natural silicic magmas using lessons learned from experiments on the Qz-Ab-Or system. Here we present a simple empirical procedure to eliminate quantitatively the effects of An on the position of normative melts in the Qz-Ab-Or ternary.

The system Ab-An-Qz is well constrained experimentally, as are the ternary feldspars (Ab-Or-An). Addition of An considerably reduces silica activity in a granitic melt, such that with increasing An the quartz phase volume contracts. Similarly, An stabilises plagioclase feldspar at the expense of K-feldspar. The effect of An on phase relations along the Oz-Or join is less well understood, because of relatively few experiments in this system, and the doubts raised by Johannes (1980) about equilibrium in some of the An-bearing experiments of Winkler and co-workers. However, all of the extant data on Qz-Or-An, including Winkler and Ghose (1973) and James and Hamilton (1969), suggest that An has a relatively modest affect on the Qz:Or ratio along the silicafeldspar cotectic, apparently shifting it to slightly higher Qz. Finally, with increasing An content at 100 MPa, water-saturated, the piercing point on the projected Qz-Ab-Or plane shifts towards the Qz-Or join (James and Hamilton 1969).

All of the information available on the effect of An on water-saturated phase relations in the system Qz–Ab–Or can be used to develop a modified projection scheme to correct for the presence of a small amount (<20%) of normative An. We have done this using the following sets of water-saturated experiments: Qz–Ab–An at 200 MPa (Holtz et al. 1992a) and at 500 MPa (Yoder

1968); Qz–Or–An at 100 MPa (James and Hamilton 1969); Ab–Or–An at 100 MPa (Elkins and Grove 1990) and 500 MPa (Yoder et al. 1957). The shifts are monitored relative to the An-free data of Bowen and Tuttle (1950), Tuttle and Bowen (1958) and Morse (1970). To ensure that the apices of the Qz–Ab–Or ternary do not shift, and that compositions along the constituent binaries do not stray into the ternary, we fitted the An-bearing data to the following expressions:

$$Qz' = Qz_n \times (1 + aAn + b[Or_n \times An] + c[Ab_n \times Or_n \times An])$$

$$Or' = Or_n \times (1 + dAn + e[Qz_n \times An] + f[Ab_n \times Qz_n \times An])$$

where the prime denotes the revised ternary co-ordinates, all units are expressed in weight percent, and the subscript n denotes that Qz, Ab and Or are first summed to 100%. Because of closure (summation to 100%) only two parameters are required to define each ternary composition, so that no correction was necessary for Ab (i.e. Ab' = 100 - Qz' - Or'). Parameters a-f were obtained by trial and error, starting with the quartz-feldspar cotectic in Qz-Ab-An, for which there are most data, followed by the two-feldspar cotectic in Ab-Or-An, and concluding with piercing points in Qz-Ab-Or-An. Parameter f was found to be unnecessary, and the following expressions were obtained:

$$Qz' = Qz_n \times (1 - 0.03An + 6 \times 10^{-5} [Or_n \times An] + 10^{-5} [Ab_n \times Or_n \times An])$$
 (1)

$$Or' = Or_n \times (1 - 0.07An + 10^{-3} [Qz_n \times An])$$
 (2)

$$Ab' = 100 - Qz' - Or' \tag{3}$$

These expressions match the co-ordinates of cotectics and piercing points from An-bearing (≤ 20% An) and An-free experiments to within ± 2 wt% Qz' and ± 4 wt% Or', which in many cases is comparable to the experimental uncertainty on the location of the phase boundary. Interestingly, although the data of Winkler et al. (1975) on the system Qz-Ab-Or-An were not used to derive the fit parameters, Eqs. (1), (2) and (3) also match their 500 MPa piercing points to the An-free eutectic of Ebadi and Johannes (1991) to within ± 2 wt% Qz' and ± 3 wt% Qr'. Similarly, the data of Winkler et al. (1977) on the water-saturated quartz-plagioclase cotectic in Qz-Ab-Or-An match the An-free cotectics to within ± 1 wt% Qz'. We were unable, however, to achieve similar success with the Qz-Or-An data of Winkler and Ghose (1973).

We have made no attempt to account for the effect of normative corundum (Cor) on the haplogranite system. From the 200 MPa water-saturated data of Holtz et al. (1992b) it is clear that adding Al_2O_3 to Qz–Ab–Or reduces the silica phase volume in an analogous way to An, with \sim 4 wt% reduction in Qz along the cotectic for melts with \sim 5 wt% Cor. As none of the natural data that we will be discussing in this paper are strongly peraluminous, we have not included this shift in our normalisation scheme, which is therefore not applicable to liquids with >1% Cor. We have also made no

attempt to revise temperatures in Qz–Ab–Or to account for the presence of An. However, following Johannes and Holtz (1996), we note that the effect of An on haplogranite liquidus temperatures is modest (e.g. a change in bulk composition from An₀ to An₃₀ at 200 MPa results in an \sim 30 °C increase in liquidus temperature).

As a check on the applicability of our revised projection scheme to natural metaluminous (<1% Cor) silicic magmas, we have plotted experimental data on natural feldspar + quartz-saturated, water-saturated silicic glasses. There are remarkably few such analyses in the literature, and only four data points could be found: Barclay et al. (1998) on a Montserrat andesite at 130 MPa; Rutherford and Devine (1996) on Pinatubo dacite at 220 (matrix glass) and 300 MPa; and Conrad et al. (1988) on a Taupo dacite at 1,000 MPa. To obtain the projection parameters we first normalised the glass analyses to 100 wt% anhydrous, then calculated the CIPW norm. Normative Qz-Ab-Or were normalised to 100% to give Qz_n , Ab_n and Or_n . These values, together with the original normative An, were used in Eqs. (1), (2) and (3) to obtain Qz', Ab' and Or'. The projected values before (Qz, etc.) and after (Qz', etc.) modification are shown in Fig. 3. After modification all four glass analyses lie very close to the Qz-Ab-Or quartz-feldspar cotectic at the appropriate pressures, whereas before normalisation this is not the case.

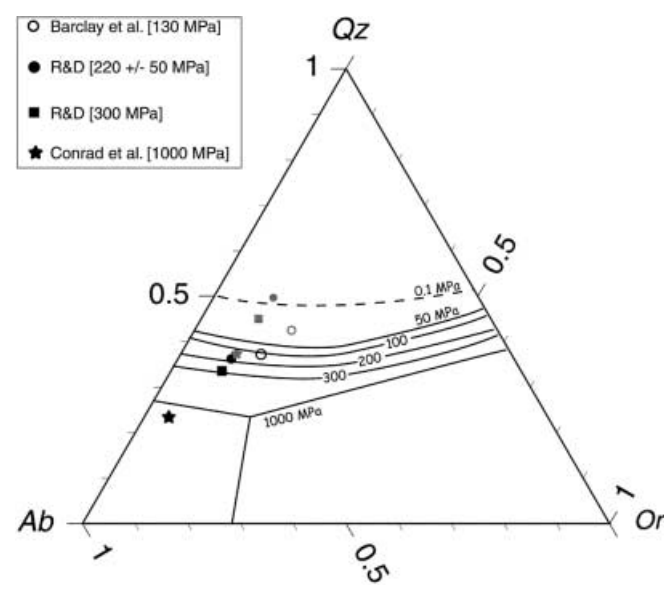


Fig. 3 Comparison of uncorrected (*small grey symbols*) and corrected (*large black symbols*) glass analyses from experiments on natural samples performed under water-, feldspar- and quartz-saturated conditions. Location of cotectics from Fig. 1. Data from Conrad et al. (1988), Rutherford and Devine (1996; R&D), Barclay et al. (1998). Uncertainties on projected Ab', Or', and Oz', from equation (1) are hard to estimate precisely because of potential problems of Na-loss during EMP analysis, and uncertainties in the projection parameters. However, from normal error propagation we calculate that typical uncertainties in SiO₂, Al₂O₃, Na₂O and K₂O, based on multiple analyses of quenched glass, translate into uncertainties of 1–2% Ab' and 0.5–2% Or' and Oz'

As a further test of both our normalisation scheme and its applicability to the crystallisation of natural silicic melts, we have calculated Qz', Ab' and Or' for published experimental glasses obtained under pressure—temperature (P-T) conditions that mimic the three end-member cases illustrated in Fig. 2. In all three cases we have selected data from experiments on Mount St Helens tephras. Results are shown in Fig. 4a–c, where they are compared with the theoretical trends presented in Fig. 2.

Water-saturated isobaric cooling (Fig. 4a)

Data were taken from the 200 MPa water-saturated experimental study of Geschwind and Rutherford (1992) on a cummingtonite-bearing Yn dacite from Mount St Helens (MSH). As full glass analyses are not reported by Geschwind and Rutherford, we used an empirical calibration of Qz' with wt% SiO₂ and Or' with K₂O from experiments and natural glasses on other MSH samples to derive plotting parameters from the data presented in their Fig. 2. Glass analyses obtained from experiments at 200 MPa over the temperature range 890–770 °C define a trend that matches that in Fig. 2a, except that the temperature is above the Qz–Ab minimum temperature at this pressure, i.e. 750 °C (Tuttle and Bowen 1958). Consequently, the melts never attain quartz saturation at the cotectic.

Water-saturated isothermal decompression (Fig. 4b)

Data were taken from the experimental study of Gardner et al. (1995) on an MSH Wn dacite. Water-saturated experiments were performed at 875 °C and 250, 150, and 100 MPa. The experimental glasses follow a track parallel to the theoretical trend, but displaced to Or-poor compositions, consistent with the Or-poor nature of the starting material (relative to Qz₁₆Ab₇₅Or₉) and the slightly higher experimental temperature (875 versus 800 °C). Once again, quartz is lacking from any of the experimental glasses, and consequently they fall short of the cotectic at all pressures. [Interpolation of Tuttle and Bowen's (1958) experimental data on the water-saturated Qz–Ab join and the water-saturated ternary minimum suggest that at 875 °C quartz would not saturate in this composition until ~60 MPa.]

Water-undersaturated isothermal decompression (Fig. 4c)

Data were taken from the experiments of Rutherford et al. (1985) and Geschwind and Rutherford (1995) on MSH sample SH-084, a white dacite pumice from the 18 May 1980 eruption. The former data were obtained at 905 ± 15 °C over pressures of 215–125 MPa, with a water content of 4.8 ± 0.1 wt% H₂O. The latter data derive from decompression experiments at 900 °C on

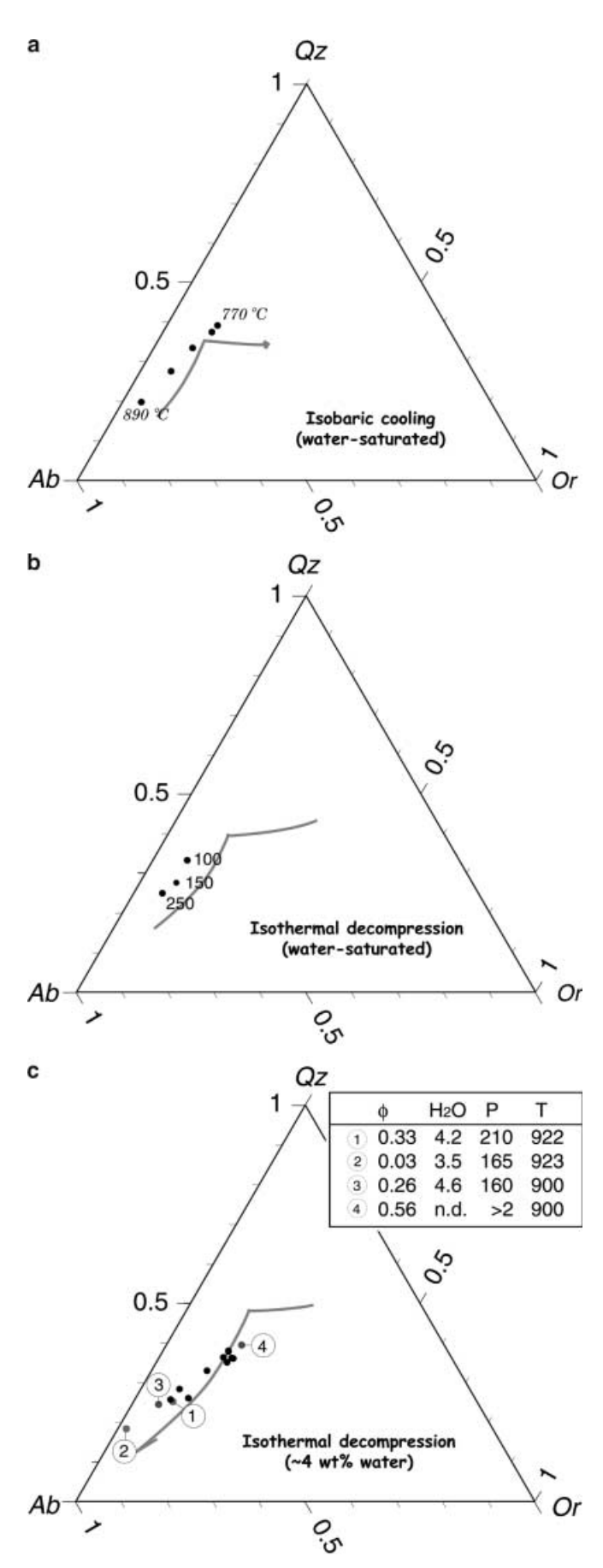


Fig. 4 Glass compositions from experimental samples of Mount St Helens pumice crystallised under different conditions. Grey lines refer to corresponding crystallisation paths shown in Fig. 2. a Water-saturated isobaric cooling at 200 MPa (Yn pumice, from Geschwind and Rutherford 1992). b Water-saturated isothermal decompression at 875 °C from 250 to 100 MPa (Wn pumice, from Gardner et al. 1995). c Water-undersaturated decompression of 1980 pumice (from Rutherford et al. 1985; Geschwind and Rutherford 1995). Data on crystallinity (ϕ) , H₂O-content, pressure (P in MPa) and temperature (T in °C) of selected grey points (identified by number) provided in inset table. Crystallinity is estimated by comparison of K₂O in the glass and bulk rock, assuming that K₂O is perfectly incompatible

a water-saturated sample over the pressure range 200-2 MPa or160-2 MPa for a variety of decompression rates. The slower the decompression rate, the closer the glass composition is to the final equilibration pressure (2 MPa). Thus the Geschwind and Rutherford (1995) glass data cover a wide range of Qz' contents, corresponding to a pressure range of 200 or 160 (fastest decompression rate) to 2 MPa (slowest decompression rate), and therefore justify comparison with our constant-water content fractionation path (Fig. 2c). The results (Fig. 4c) show a remarkably faithful coherence with the calculated trend. Glass compositions initially track towards the Ab apex because of feldspar resorption at pressures of 220 to160 MPa. They subsequently migrate rapidly towards the (inferred) 0.1 MPa cotectic. The authors do not report if quartz or tridymite was found in any of the run products. Our calculations based on the water-saturated Qz-Ab binary suggest that at 900 °C quartz should occur in runs with a final (effective) equilibrium pressure of 40 MPa or less.

Overall, Fig. 4a–c supports our contention that both decompression crystallisation and cooling crystallisation drive melts towards the Qz apex. The trend for both cases is sub-parallel, but once again we emphasise that high Qz contents can only be attained if the final crystallisation pressure, and hence dissolved H₂O content, is low.

The data of Geschwind and Rutherford (1995) further illustrate the important role of ascent (decompression) rate on the extent to which equilibrium is achieved. Cashman and Blundy (2000) discuss in detail the effect of decompression rate on glass composition by defining a closure pressure (Pc) at which kinetic factors inhibit further crystal growth and melt chemistry is frozen-in. For a series of magmas ascending from a given source region (say at 200 MPa), the magmas that ascend the most rapidly will record the highest value of P_c, which in the case of very rapid ascent will approach 200 MPa. Conversely, very SiO₂-rich melts, corresponding to low values of P_c, can only be produced in magmas that have experienced slow ascent or temporary near-surface arrest prior to eruption. For water- and quartz-saturated silicic melts P_c can be determined simply by projecting the glass composition on the Qz-Ab-Or ternary (Fig. 1). Where quartz (or tridymite) is not a crystallising phase, projection of glass compositions onto Fig. 1 only allows determination of relative values of P_c.

From this discussion it is evident that, in theory at least, the decompression and cooling history of ascending silicic melts, and the distribution of magma arrest levels within the sub-volcanic system, can be constrained solely from major element glass data. In the following section we apply this methodology to groundmass and inclusion glasses from the 1980–1986 eruption of Mount St Helens.

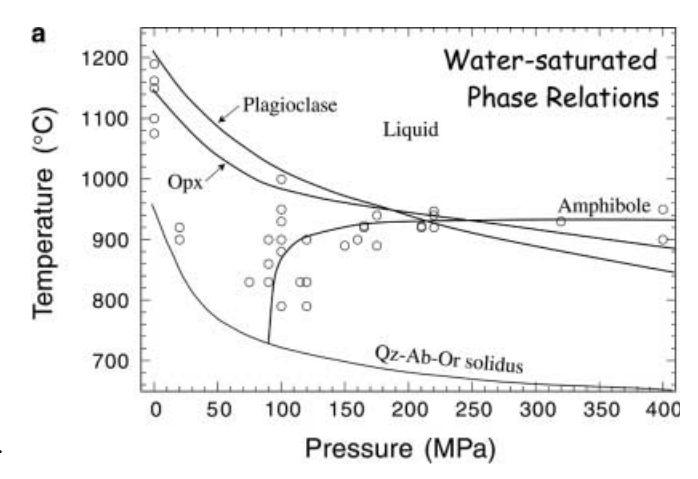
Mount St Helens – previous studies

Reviews of the magmatic history and petrogenetic processes at Mount St Helens (MSH) volcano can be found in Pallister et al. (1992) and Gardner et al. (1995). Magma produced during the most recent eruption of Mount St Helens (1980–86) is porphyritic dacite with 63–64 wt% SiO_2 and phenocrysts of plagioclase, amphibole, orthopyroxene and Fe–Ti oxides (Cashman and Taggart 1983). Oxide thermometry yields pre-eruptive temperatures of $900\pm10\,^{\circ}\mathrm{C}$, for almost the entire duration of the eruption (Rutherford and Hill 1993).

Experimental phase relations of a 18 May 1980 dacite have been determined for water-saturated and waterundersaturated conditions by Merzbacher and Eggler (1984), Rutherford et al. (1985), Rutherford and Devine (1988) and Rutherford and Hill (1993). Data for the water-saturated case are summarised in Fig. 5a, which shows several key features of importance to the process of decompression crystallisation in natural magmas. Firstly, liquidus temperatures increase rapidly with decreasing pressure, in accord with the pressure dependence of water solubility. Secondly, the liquidus phase changes from plagioclase at low pressure, to orthopyroxene at \sim 200 MPa, to amphibole at higher pressures. (Saturation curves for clinopyroxene and oxides, which depend critically on f_{O2} , are omitted from Fig. 5a for clarity.) Finally, amphibole, which requires ~4 wt% water dissolved in the melt in order to crystallise (Merzbacher and Eggler 1984), is not stable below 150 MPa at 920 °C and below 100 MPa at 880 °C.

In Fig. 5b we illustrate an important feature of magma ascent at MSH and other silicic volcanoes, namely the relationship between the liquidus curve and the ascent path of the magma. The divergence between the two defines an undercooling driving force (ΔT) for crystallisation, whose magnitude depends on ascent rate. Thus magma that ascends very slowly and isothermally from 220 MPa will generate considerably less undercooling than magma that ascends rapidly. Large undercooling is associated with increased nucleation rate, whereas small undercooling favours increased growth rate. In the extreme case, ascent is too rapid (ΔT too high) for crystallisation to occur, and the magma crosses the glass transition temperature before any crystals can form (Cashman and Blundy 2000).

For the purposes of our discussion of glass chemistry at Mount St Helens, consider a volatile-saturated dacite magma that is at its liquidus at 220 MPa just prior to ascent. For simplicity (and because there are



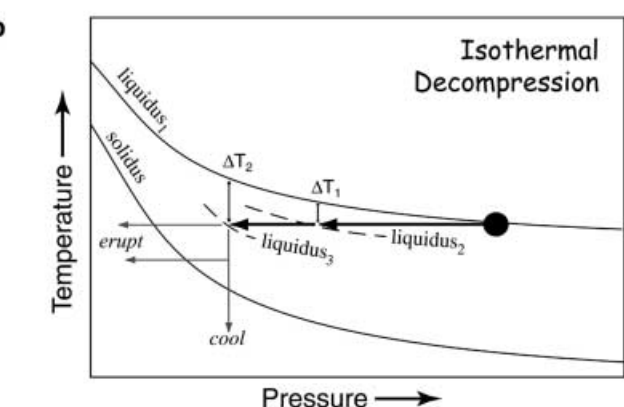


Fig. 5 a Summary water-saturated phase diagram for Mount St Helens 1980-86 dacites from experimental work of Merzbacher and Eggler (1984), Rutherford et al. (1985), Rutherford and Devine (1989), Rutherford and Hill (1989). Open circles denote experimental data points used to construct the diagram. Note the sharp increase in liquidus temperature and the changing nature of the liquidus phase with decreasing pressure. Saturation curves for Fe-Ti oxides and clinopyroxene have been omitted for clarity. Fe-Ti oxide saturation depends on f_{O2} , but at NNO lies close to orthopyroxene saturation. Note also the stability field of amphibole, and its sensitivity to temperature in the pressure range 100-160 MPa. Amphibole is not stable at any temperature below ~95 MPa. **b** Schematic isothermal decompression path for a Mount St Helens dacite showing two ascent steps from a deep magma reservoir, each associated with an undercooling, ΔT₁ and ΔT_2 , relative to the liquidus at the appropriate pressure. The magnitude of ΔT determines the abundance and texture of crystals. Where ascent is rapid and/or shallow large ΔT results, promoting crystal nucleation; for slow and/or deep ascent small ΔT results, promoting crystal growth (Cashman and Blundy 2000). Note, that in drafting this figure we have assumed that after each ascent step there is sufficient time for crystallisation to reduce the liquidus to the isotherm (i.e. $liquidus_{1-3}$). This may or may not be the case in nature. After the second ascent step we show that the magma may either erupt immediately, or cool slightly before eruption, as indicated by the arrows

more experimental data) we will consider a pure H₂O volatile phase. However, we would arrive at broadly similar conclusions in the case of a mixed-volatile phase (e.g. C–H–O–S), as proposed by Rutherford et al. (1985) and Rutherford and Devine (1988). In practice we can envisage ascent of this magma as a series of near-isothermal steps, each generating an

undercooling (ΔT) that drives crystallisation until the magma is once again at its liquidus (Fig. 5b). Release of latent heat of crystallisation en route may in fact increase temperature during ascent, whereas magma arrest may lead to heat loss to wall rocks, and temperature drop during ascent. In any case it is clear that the P–T-time path followed by individual magma batches will control the resulting phase assemblage, chemistry and groundmass texture (e.g. Cashman and Blundy 2000). Therefore by carefully examining textures and relating them to glass chemistry, it is possible to reconstruct magma movement through the conduit-reservoir system beneath the volcano. We will do this first for groundmass glasses, and then for glass inclusions in phenocrysts.

Glass analyses are available for samples from all phases of the 1980–1986 activity (e.g. Scheidegger et al. 1982; Melson 1983; Rutherford et al. 1985; Cashman 1992; Geschwind and Rutherford 1995). In addition, new glass analyses (Table 1) were obtained for three further MSH samples: SH 133, a Peleean spine, previously described by Cashman (1992); SH149, a sample of the active 'mound' that characterised endogenous activity at Mount St Helens throughout 1983; and SH80D, a porphyritic grey dacite pumice (density = 1.58 g cm^{-3}) from 18 May 1980, previously described in Holten et al. (1997). Although the glass analyses come from a wide range of sources the consistency of normative compositions between different laboratories testifies to the relative insensitivity of our methodology to analytical protocols. Undoubtedly some analyses have suffered Na-loss more acutely than others, but this is not manifest in our

Table 1 Electron microprobe analyses of samples where compositions are not reported elsewhere in the literature. Columns 1–3 report new glass data for 18 May 1980 grey dacite sample SH80D (Holten et al. 1997) and endogenous dome samples SH133 and SH149 (Cashman 1992). Columns 4–5 present analyses of groundmass tridymite and quartz in sample SH149

Column Sample	1 SH80D g-mass	2 SH149 g-mass	3 SH133 g-mass	4 SH 149 Tridymite	5 SH 149 ite Quartz	
SiO ₂	77.04	80.63	79.59	97.79	100.44	
TiO_2	0.36	0.30	0.28	0.10	0.03	
Al_2O_3	12.45	11.01	11.09	1.99	0.64	
FeO	1.47	1.29	1.37	0.16	0.12	
MnO	n.d.	0.02	0.04	0.00	0.02	
MgO	0.25	0.09	0.06	0.02	0.01	
CaO	0.88	0.33	0.23	0.07	0.11	
Na ₂ O	3.74	3.02	2.74	0.55	0.22	
K_2O	3.17	4.22	5.32	0.52	0.04	
Total	99.37	100.89	100.73	101.19	101.61	
Normalis	ed					
SiO_2	77.53	79.92	79.01	96.64	98.84	
TiO_2	0.37	0.29	0.28	0.09	0.03	
Al_2O_3	12.53	10.91	11.01	1.97	0.63	
FeO	1.48	1.28	1.36	0.16	0.11	
MnO		0.01	0.04	0.00	0.01	
MgO	0.25	0.09	0.05	0.01	0.01	
CaO	0.88	0.32	0.23	0.07	0.11	
Na ₂ O	3.76	2.99	2.72	0.54	0.22	
K_2O	3.19	4.18	5.28	0.51	0.03	

projection schemes (as we omit analyses with extreme Na-loss and correspondingly high normative Cor; Merzbacher and Eggler 1984). Typical analytical uncertainties on oxide concentrations in natural glasses as measured by EMPA propagate to ± 0.5 –2% Qz' and Or', and ± 1 –2% Ab'. We conclude that our observations and deductions are not a consequence of analytical artefact.

1980–1986 eruption of Mount St Helens – matrix glass composition

The 1980–1986 eruption of Mount St Helens was initiated on 18 May 1980 with failure of the mountain's unstable north flank accompanied by a lateral blast, and followed by 9 h of sub-Plinian to Plinian explosive activity (e.g. Lipman and Mullinaux 1981). The instability of the north flank was a consequence of the intrusion of a dacite cryptodome high in the volcanic edifice during the 2 months prior to the eruption. Pyroclastic deposits from 18 May preserve both white pumice from the Plinian activity and dense grey dacite from the cryptodome, thus allowing comparison of samples that experienced temporary pre-eruptive storage at different levels within the reservoir-conduit system prior to 18 May (e.g. Fig. 6a, b). Subsequent to May 1980, explosive eruptions occurred at decreasing intensities through the summer of 1980 (Scandone and Malone 1985), and by late 1980 activity was almost exclusively effusive (e.g. Swanson et al. 1987). Explosive activity continued sporadically throughout the summer of 1980, with explosive activity waning by December 1980, by which time the eruption was dominated by effusive activity (e.g. Scandone and Malone 1985; Swanson et al. 1987; Fig. 6c-h). Effusive activity persisted until 1986, but varied from exogenous, with the emplacement of discrete lava lobes, to endogenous dome expansion accompanied by occasional spine extrusion.

18 May 1980 pumice

Most samples produced during the vigorous eruption of 18 May 1980, are low density, microlite-free white pumice (Criswell 1987; Klug and Cashman 1994; Fig. 6a). The magma is dacitic (63% SiO₂), with $\sim 30\%$ phenocrysts of amphibole, plagioclase, orthopyroxene, Fe–Ti oxides and rare clinopyroxene (Kuntz et al. 1981). Experiments suggest that the matrix glass was last in equilibrium with the observed phenocryst rim compositions at 220 MPa and 900-920 °C (Rutherford et al. 1985; Rutherford and Devine 1988; Rutherford and Hill 1993). The best match of experimental and matrix glass was obtained for water-undersaturated conditions (fluid $X_{H,O} \approx 0.67$), a finding in keeping with the low water content of plagioclase-hosted glass inclusions $(4.6 \pm$ 1.1 wt%) compared with the saturation value at 220 MPa, 900 °C of 6.2 wt% (Moore et al. 1998). Estimates of the pre-eruptive volatile content of Mount St Helens 1980–86 magmas derive exclusively from

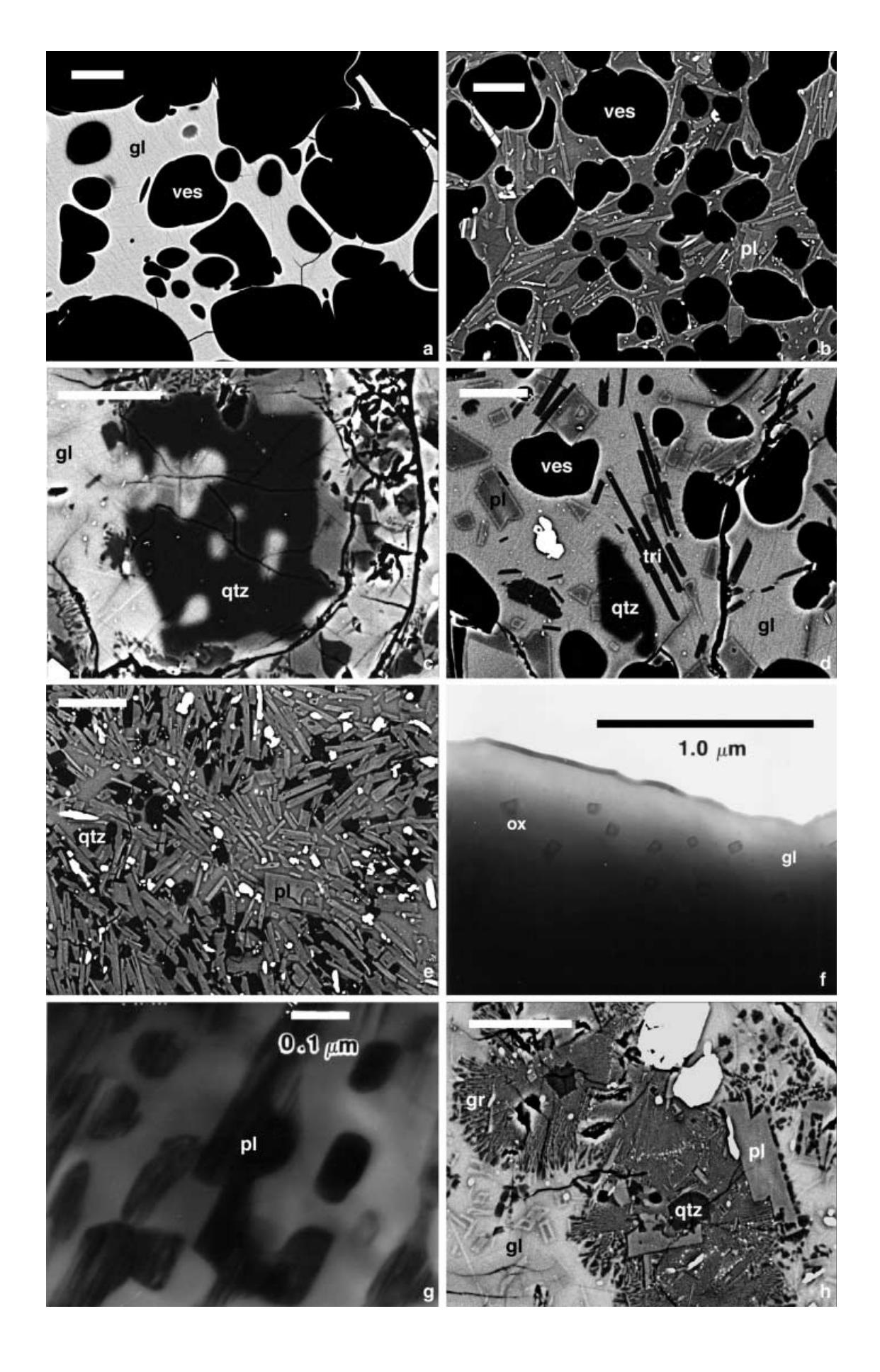


Fig. 6 Backscattered electron (BSE) and TEM images of Mount St Helens samples. *Scale bars* are 10 μm except where labelled. **a** BSE image of pumice sample T8 W erupted 18 May 1980 consists of microlite-free glass (*gl*) and vesicles (*ves*). **b** Grey pumice sample T8G erupted 18 May 1980 contains plagioclase (*pl*) microlites in addition to glass and vesicles. **c** Microlite of resorbed quartz (*qtz*) in endogenous dome sample SH146 erupted 2/83. **d** Tridymite (*tri*)bearing endogenous dome sample SH149 erupted 2/83. **e** Blast dacite sample BD8 contains aligned plagioclase and poikilitic quartz in the groundmass; erupted 18 May 1980. **f** TEM image of oxides (*ox*) in K-rich glass from dome interior sample SH53, erupted 10/80. **g** TEM image of feldspar—quartz intergrowths in groundmass SH53. **h** BSE image of graphic textures (*gr*) forming spherulitic intergrowths in SH53. Samples described in Cashman (1992), Klug and Cashman (1994)

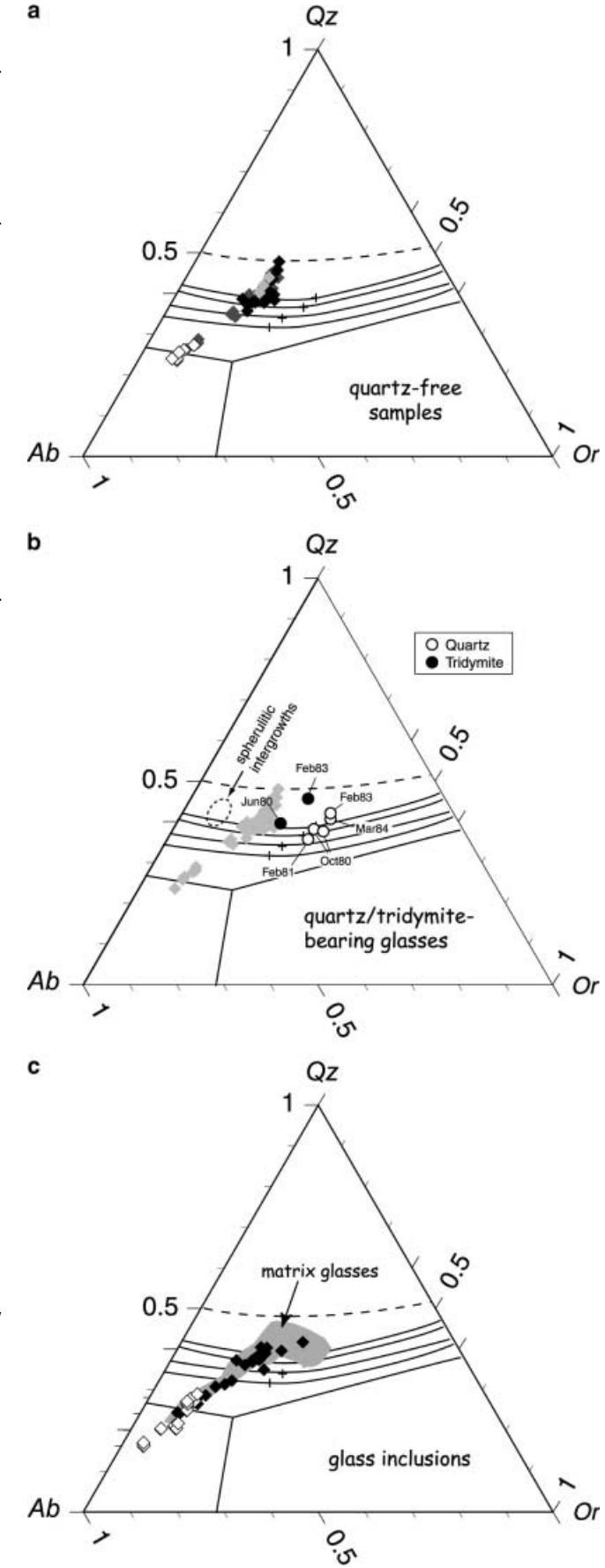
electron microprobe analyses of glass inclusions using the 'by difference' method, which is subject to an uncertainty of ± 0.7 wt% (Devine et al. 1995). To date there are no direct measurements, for example by FTIR or ion-microprobe, of H_2O or other volatiles in glasses from this eruption. These conditions correspond to a magma storage region at ~ 8.5 km depth prior to the 1980–1986 eruption. In this study all depths at Mount St Helens were calculated using the density model of Williams et al. (1987). Note, that at 900 °C a dacite magma with 4.6 wt% dissolved H_2O would not become water saturated until reaching a pressure of ~ 150 MPa (Moore et al. 1995).

The rhyolitic matrix glass (73% SiO₂; Rutherford et al. 1985) projects to the Qz-poor side of the 200-MPa water-saturated cotectic (Fig. 7a). The absence of phenocrystic quartz, together with the location of glass compositions near the Ab apex of the Qz–Ab–Or ternary, indicate that the high temperature of the melt prevented it from reaching the 200-MPa quartz–feldspar cotectic.

18 May 1980 cryptodome samples

As noted by Hoblitt and Harmon (1993), the blast deposit contains abundant grey dacite clasts of both

Fig. 7 Projection of natural MSH 1980–86 glass compositions onto Qz-Ab-Or ternary; cotectic lines and compositions of minimum melts from Fig. 1. a Groundmass glasses from quartz(or tridymite)free samples from 18 May 1980 white pumice (open diamonds) and grey pumice (light grey diamonds); summer 1980 pumices (medium grey diamonds); and 1980-1986 effusive rocks (filled diamonds). Data from Scheidegger et al. (1982), Melson (1983), Cashman (1992), Geschwind and Rutherford (1995). b Groundmass glasses from quartz-bearing (open circles) and tridymite-bearing (filled circles) samples from spine and dome samples from 1980-1986. Analyses and sample descriptions can be found in Cashman (1992) and Table 1. Also shown is the compositional field of spherulitic intergrowths in spine and dome interior samples (from Cashman 1992, reported there as 'dark' glasses), and the field of quartz-free groundmass glasses from b. c Compositions of melt inclusions in amphibole (open symbols) and plagioclase (filled symbols) phenocrysts; compositional field of matrix glasses shown for comparison (shaded region). Data from Melson (1983), Rutherford et al. (1985), Rutherford and Devine (1988), Table 1, and Cashman (unpublished data)



intermediate and high densities that are pieces of the cryptodome intruded prior to 18 May 1980. Cryptodome dacite samples are highly crystalline (Fig. 6b), with abundant small (<10 μm) plagioclase laths surrounded, in places, by poikilitic quartz. Although the plagioclase laths commonly exhibit a strong preferred orientation, mostly likely a consequence of flow related to cryptodome emplacement, the lack of any apparent preferred orientation of the quartz poikilocrysts suggests that magma movement ceased at or before quartz saturation. Glass compositions can be measured only in the least crystalline samples, and are highly evolved (>79% SiO₂), projecting onto the Qz–Ab–Or ternary diagram between the 50 and 0.1 MPa cotectics (Fig. 7a). As quartz is a precipitating phase, the projection of these compositions records the actual pressure (depth) of crystallisation as long as equilibrium was attained, e.g. quartz was not supersaturated.

Summer 1980 explosive deposits

Explosive eruptions continued episodically through October 1980. Although the magma composition remained fairly constant, pumiceous clasts from deposits generated during these events vary in colour (Lipman et al. 1981), density (Kuntz et al. 1981), and groundmass crystallinity (Cashman and Blundy 2000). Changes in groundmass glass composition accompany textural changes, as illustrated by projection of glass compositions onto the Qz-Ab-Or ternary (Fig. 7a). Low density white pumiceous samples lack microlites and have compositions that plot in the same location as pumiceous samples from 18 May (Fig. 7a). In contrast, higher density grey pumice samples (Fig. 6c) show varying amounts of microlite crystallisation, and have glass compositions that are correspondingly evolved. Projection of these compositions onto the Qz-Ab-Or ternary shows a trend away from Ab toward the 0.1 MPa cotectic, and parallel to the depressurisation trend of the ternary minimum (Fig. 2b). These samples only rarely contain quartz or tridymite, thus the observed compositional range implies only that crystallisation occurred at a range of effective pressures. Nonetheless, given the high SiO₂ content of the most evolved glasses some crystallisation must have occurred at very shallow levels within the conduit (e.g. Cashman and Blundy 2000).

1980–1986 effusive activity

Effusive eruption of dacitic lava continued from late 1980 through 1986. The beginning and ending phases of dome growth (1980–1982 and 1984–1986, respectively) were episodic and exogenous, with discrete flow lobes added to the growing central dome. In contrast, effusion was continuous throughout 1983, with dome growth during that period primarily endogenous. Lava samples collected hot from actively growing dome lobes have

homogeneous matrix glass that contains microlites of plagioclase, orthopyroxene, and Fe–Ti oxides, but no quartz or tridymite. Glass analyses from these samples have normative compositions that project onto the Qz–Ab–Or ternary in a linear trend away from Ab (Fig. 7a), similar to the trend observed in samples from the summer of 1980. The only difference between the dome dacites and those erupted explosively is that the dome samples have a more restricted range in glass composition, with most glasses plotting to the Qz-rich side of the 50 MPa cotectic. These evolved glass compositions indicate extensive plagioclase crystallisation at low pressure (≥50 MPa).

Lava dome samples that experienced slow ascent during the endogenous phase of dome growth and/or protracted cooling in the dome interior have complex groundmass textures. The microlite assemblage includes high-silica glass and microlites of plagioclase, orthopyroxene, Fe-Ti oxides and a silica mineral. This is typically quartz, but may (rarely) also include tridymite (Fig. 6d). Quartz occurs in two forms, either as discrete microlites that are rounded and embayed (Fig. 6e) or as poikilocrysts, as seen in the cryptodome dacite (e.g. Fig. 6b). Where present tridymite forms acicular laths, a habit distinct from the vapour phase tridymite documented in cryptodome samples by Hoblitt and Harmon (1993). However, we note that if vapour and melt coexist in equilibrium, then tridymite saturation will occur simultaneously in both phases. In this context it is interesting to note that the thermodynamic gas-phase calculations of Symonds and Reed (1993) predict that volcanic gases emitted from the Mount St Helens dome in September 1981 are in equilibrium with beta-tridymite at 930 °C and pressures of 0.1 to 10 MPa, but with beta-quartz at 710 °C and 0.1 MPa. This finding is consistent with the presence of tridymite in some dome samples, and our independent estimates of the P-T conditions at which it formed (see below).

Finally, some samples of extruded spines or of the slowly cooled dome interior have matrix glass that appears heterogeneous on a scale of 10 to 100 s of microns (Cashman 1992; her Fig.7), a texture originally interpreted by Cashman as post-extrusion crystallisation or devitrification. Examination of these 'glasses' using TEM imaging indicates that while the high-K variety are true glasses with small Fe-oxides (Fig. 6f), the Na-Ca variety are finely crystalline intergrowths of feldspar and quartz (Fig. 6g). High-resolution backscattered electron (BSE) images show that such quartz-feldspar intergrowths form spherulites (Fig. 6h). Such textures are characteristic of cotectic precipitation from highly viscous melts (e.g. Fenn 1977).

Pressure and temperature estimates

The presence of quartz and/or tridymite, and the composition of coexisting groundmass glasses in

cryptodome, dome interior and spine samples can be used to infer crystallisation pressure and temperature (Fig. 8). If vapour pressure and lithostatic pressure are approximately equal, i.e. there is limited overpressure, then calculated pressures can be converted into depths. Quartz-bearing glasses from spine and dome interior samples have compositions that lie close to the watersaturated minimum at apparent pressures of ~ 30 to slightly over 100 MPa (Fig. 7b). Migration of glass compositions along cotectic boundaries is consistent with evidence for co-precipitation of quartz and feldspar, and suggests that samples containing intergrowths underwent isobaric cooling in a shallow reservoir or within the magmatic conduit. Quartz-saturation temperatures have not been determined experimentally for MSH samples, but may be estimated at 780–860 °C from the minima of Tuttle and Bowen (1958), with allowance for an anticipated 30 °C increase in temperature because of ~30 mol% added An (Johannes and Holtz 1996). As the magma was erupted at 900-920 °C (Rutherford and Devine 1988), cotectic crystallisation under near-surface conditions appears to have been aided by cooling. Glass in the tridymite-bearing sample from the endogenous phase of dome growth (February 1983) is also Qz'-rich, consistent with equilibration at very low pressure (Fig. 7c). In the An-free system the water-saturated silica-feldspar cotectic intersects the high quartz-tridymite phase boundary (Tuttle and Bowen 1958) at a minimum P and T of 11 MPa and 885 °C, respectively. The maximum values of pressure and temperature of crystallisation are less well defined. However, if we assume that the presence of An₃₀ in groundmass plagioclase (Cashman 1992) elevates temperatures along the silicafeldspar cotectic by ~30 °C, then maximum P and T values of 25 MPa and 915 °C, respectively, are obtained (Fig. 8). Additionally, as tridymite has lower SiO2 and higher Al₂O₃ than coexisting quartz (Table 1), the tridymite-quartz phase boundary in natural systems will be shifted to still higher T than in the pure SiO₂ system. In any event, the similarity of our minimum and maximum T estimates to the temperature in the magma chamber is strongly suggestive of near-isothermal magma ascent and crystallisation at very shallow levels (1200-500 m). Rutherford and Hill (1993) arrive at a similar conclusion, based on oxide thermometry of cryptodome grey dacites (which may also contain tridymite - see above), which gives temperatures of 875 ± 15 °C, compared with 895 ± 15 °C for the white dacite erupted later that on 18 May.

The dacite magmas appear to have crystallised over a large effective pressure range (Fig. 8). This suggests either that during some dome eruptions ascent from the deep, ≥6 km, reservoir was too rapid to permit full re-equilibration, or that some dome-forming magma was stored at shallow levels (<6 km) prior to eruption. Distinguishing between these rival, but not mutually exclusive, hypotheses has important implications for magma dynamics at MSH. Germane to this discussion is the amphibole breakdown studied experimentally by

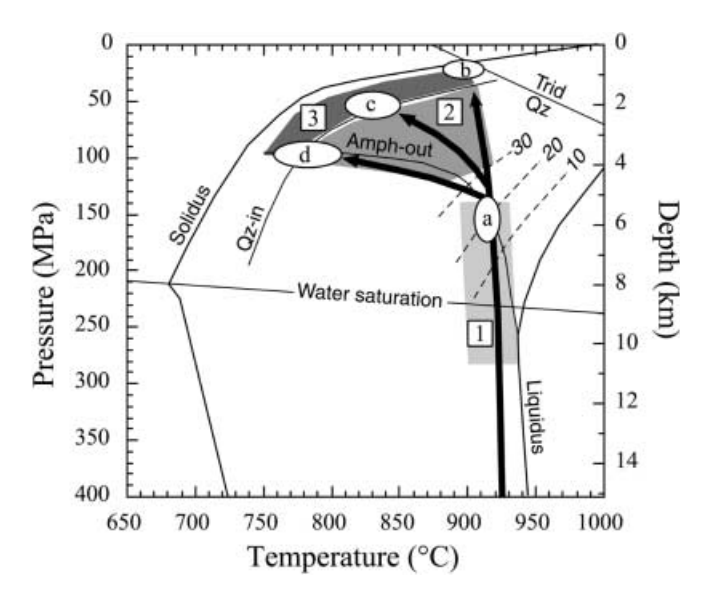


Fig. 8 Magma ascent and crystallisation history of Mount St Helens 1980–1986 as proposed in this study, cf. Fig. 3 of Rutherford and Hill (1993). The phase diagram is drawn for MSH dacite with a fixed water content of ~ 6 wt%. Liquidus phase relations at pressures $< \sim 220$ MPa from Fig. 5a; higher pressure phase relations are based on the water undersaturated experiments of Merzbacher and Eggler (1984), Rutherford et al. (1985) and Rutherford and Devine (1988). The water-saturated solidus has been modified slightly from that in Fig. 5a to allow for $\sim 30\%$ An component in the system Qz-Ab-Or-An-H₂O (Johannes and Holtz 1996); the water undersaturated solidus is partially schematic. The quartz (Qz) saturation curve, which has not been determined experimentally, is based on inferences from synthetic systems (Johannes and Holtz 1996), and is probably accurate to no better than ± 30 °C. The quartz-tridymite (Trid) phase transformation is taken from Tuttle and Bowen (1958). Thin curves labelled 10, 20, 30 denote per cent crystallinity (assuming that no crystals were present at the point of water saturation) calculated by mass balance from phase compositions in Rutherford et al. (1985; Table 2), and from Fig. 2 of Merzbacher and Eggler (1984). The heavy, arrowed lines denote selected ascent paths of magmas. Shaded regions 1–3 denote different crystallisation assemblages and/or textures; ellipses a-d denote magma storage levels. Phenocryst crystallisation, first water undersaturated (P> 230 MPa), with the precipitation of amphibole and possibly orthopyroxene; then water saturated (P≤ 230 MPa), up to crystallinities of $\sim 30\%$; 2 plagioclase \pm orthopyroxene microlite crystallisation, possibly accompanied by zoning overgrowth of phenocrysts, during further ascent over a wide P-T range; 3 stability field of quartz microlites and/or spherulitic textures. a Deep reservoir containing porphyritic, microlite-free amphibole-bearing dacite, directly sampled during Plinian phase of 18 May 1980 eruption. Magma is supplied from this region to shallow levels in the sub-volcanic system. b Cryptodome storage region during spring 1980. Some tridymite-bearing magma involved in February 1983 dome eruptions may also have been stored at this level. Amphibole is unstable. c Shallow storage of dome-forming magmas, e.g. February-March 1983. At pressures of ~50 MPa, quartz saturation occurs at 850 ± 30 °C. Amphibole is unstable. d Deeper storage of dome-forming magmas, e.g. February 1981. At 100 MPa amphibole and quartz coexist at ∼780 °C

Rutherford and Hill (1993) on MSH samples. Their data show clearly that amphibole phenocrysts in magma held outside the amphibole stability field (Fig. 5a) cannot survive for more than a few days before breaking down to a reaction rim of oxides, pyroxene, plagioclase and melt. The thickness of the reaction rims observed in natural samples can therefore be used as a measure of ascent rate. As all 1980–86 eruptive products, with the exception of the white pumice from the Plinian phase of 18 May 1980, and the cooler (860 °C) dome dacites from October 1986, have amphibole reaction rims the implication is that all magmas ascended sufficiently slowly to allow amphibole breakdown to occur. In detail amphibole reaction rims vary greatly in width within individual samples, suggesting variations in ascent rate during an individual eruption, a phenomenon that Rutherford and Hill (1993) attribute to conduit flow. They further argue that all magma in the 1980-1986 eruption was supplied from the reservoir at \sim 8 km, where amphibole was a stable phase. An alternative interpretation of these data is that magma was stored at various levels within the sub-volcanic system prior to an eruption. Some magmas were stored within the amphibole stability field (e.g. trajectory d in Fig. 8), and therefore lacked reaction rims (e.g. October 1986), while other magmas were stored outside the amphibole stability field (e.g. trajectory c in Fig. 8), and developed rims, whose thickness reflects storage time prior to eruption. Variable ascent rate, and therefore variable ΔT , will also influence the grain size of the reaction rims. A single eruption might tap different magma that had previously ascended to different storage levels at different rates, so producing the mingled textures and variable rim thickness and grain size observed (Rutherford and Hill 1993). Of course, the amphiboles could then experience further breakdown during eruption, if ascent rate was sufficiently slow. Mingling of magmas from different storage levels is inevitable if the magma conduit remains full or partially full between eruptions.

Our data do not demonstrate unequivocally that there were shallow magma storage levels prior to some 1980–1986 eruptions, simply that this remains a possibility. However, there are two lines of supporting evidence for shallow magma storage subsequent to May 1980. The first comes from the P-wave seismic tomography study of Lees (1992), which clearly shows low velocity material (magma) at depths of 3.5 to 6 km below the present-day summit. Secondly, from May 1980 to October 1986, mass eruption rates declined (Scandone and Malone 1985; Endo et al. 1990; Geschwind and Rutherford 1995) and activity changed from explosive to effusive (Swanson et al. 1987). The eruptive products changed correspondingly. The groundmass crystallinity increased (Cashman 1992), with the phase assemblage dominated by plagioclase. The evolution of the matrix glass composition to high Qz' records decreasing P_c with decreasing ascent rate, consistent with the experiments of Geschwind and Rutherford (1995). All of these features suggest an upwards migration of the mean magma storage depth with time.

In summary (Fig. 8), compositional variation in groundmass glasses from the 1980–1986 eruption is consistent with ascent-driven groundmass crystallisation of water-saturated dacite magma under near-isothermal

conditions. The final pressure recorded by a particular sample is a function of ascent path, and can be deduced from glass composition. Some quartz-bearing samples apparently experienced additional crystallisation driven by isobaric cooling at shallow levels. These levels may correspond to storage regions at 2–4 and 0.5–1 km depth from which later eruptions were derived.

Glass inclusions

As many plagioclase and some amphibole phenocrysts from MSH tephras contain glass inclusions, we might expect these to tell a complementary story to the groundmass glasses regarding deeper magmatic processes. In this section we examine the compositional variation in glass inclusions using new (unpublished) and published data (Melson 1983; Rutherford et al. 1985; Rutherford and Devine 1988).

The glass inclusion analyses were converted to the parameters Qz', Ab' and Or' derived according to Eqs. (1), (2) and (3). These data are plotted in Fig. 7c, and distinguished by host phase. As previously noted by Melson (1983) and Rutherford et al. (1985), for any given sample the plagioclase-hosted glass inclusions are remarkably similar in composition, on an anhydrous basis, to their groundmass counterparts. In fact, Melson (1983) observed a strong correlation between inclusion glass and groundmass glass for samples erupted after 18 May 1980 – samples with the most evolved groundmass glass also have the most evolved inclusion glass. Melson also observed a corresponding decrease in dissolved volatile content (estimated by difference) with increasing differentiation of the inclusion glasses. This correlation, which is shown by all available glass inclusion data (Fig. 9), is strongly suggestive of water-saturated ascentdriven fractional crystallisation.

The highest volatile content determined by Melson was 7.1 wt% for glass inclusions in plagioclase from the 18 May 1980 white pumice. This value may be slightly elevated due to Na-loss during EMPA (Rutherford et al. 1985); our unpublished analyses of inclusions from the same sample give a volatiles-bydifference (VBD) value of 5.9 wt%. This value is very close to water saturation at 220 ± 10 MPa, 920 ± 5 °C, as determined experimentally (Rutherford et al. 1985; Rutherford and Devine 1988), and according to the model of Moore et al. (1995). Conversely, Rutherford et al. (1985) find that the plagioclase-hosted glass inclusions have a wide range of VBD (3.5-5.7 wt%), corresponding to saturation pressures of 75–170 MPa (again based on Moore et al. 1995). While the exact depth at which plagioclase-hosted melt inclusions reached water saturation awaits accurate direct determination of dissolved volatile content, these inclusions were plausibly entrapped within plagioclase phenocrysts under water-saturated (or near-saturated) conditions over a wide pressure range (Fig. 9). We thus propose that Mount St Helens dacite magma reached

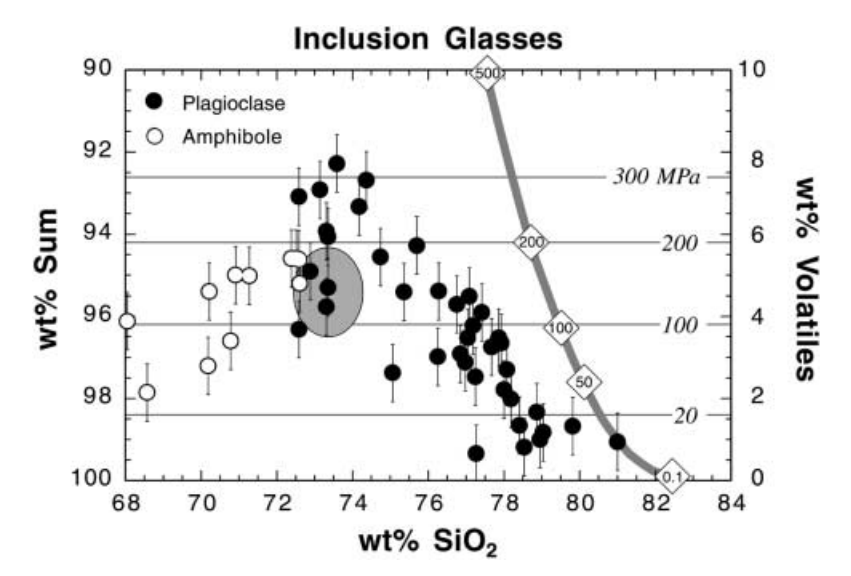


Fig. 9 Plot of volatile content (as measured by difference using EMPA) versus SiO₂ content (normalised to 100% anhydrous) of Mount St Helens glass inclusions in plagioclase (solid symbols) and amphibole (open symbols). Data are taken from Melson (1983), Rutherford and Devine (1988) and Blundy (SH80D; unpublished data). The vertical error bars denote the likely accuracy of the technique, ± 0.7 wt% (Devine et al. 1995). The large elliptical shaded region is the mean composition of plagioclase-hosted inclusions from 18 May 1980 white pumice (Rutherford et al. 1985). Horizontal lines denote saturation pressures (in MPa) for different water contents, calculated by the method of Moore et al. (1995), using 18 May groundmass glass composition. For the MSH samples the overall decrease in volatile content with increasing SiO₂ is consistent with decompression-driven crystallisation. The amphibole-hosted inclusions, although scattered, do not extend this trend to lower SiO2, suggesting that they may not have formed under volatile-saturated conditions and/or have experienced varying degrees of post-entrapment volatile loss. The open diamonds connected by the thick grey curve denote water solubilities at the haplogranite ternary minimum for different pressures, shown in MPa within each diamond (Johannes and Holtz 1996). This trend is qualitatively similar to the MSH trend, although displaced to higher SiO₂ because, with few exceptions, the natural samples are less evolved than minimum melts (Fig. 7)

water saturation at ~ 200 MPa, and that its subsequent ascent led to extensive decompression-driven crystallisation of plagioclase under water-saturated conditions. Based on our discussion of the phase assemblage and glass chemistry in some dome samples (including the cryptodome), we concur with Rutherford and Hill (1993) that magma ascent was near-isothermal, probably adiabatic. Plagioclase phenocryst growth continued to relatively low pressures, as evinced by the correlation between inclusion glass and groundmass glass compositions in dome samples (Figs. 7c and 8), and the impossibility of achieving such SiO₂-rich glasses by isobaric cooling at 220 MPa. Additional evidence of shallow phenocryst growth lies in the 2 wt% VBD determined by Melson (1983) for the most evolved glass inclusions (78.2 wt% SiO₂ in a dome lava erupted in April 1981), which corresponds to a saturation pressure of only 30 MPa (Moore et al. 1995; Fig. 9).

Glass inclusions in amphibole phenocrysts reported by Rutherford and Devine (1988) support our contention that most plagioclase growth occurred subsequent to water saturation. These glass inclusions have compositions that are significantly less evolved than those in plagioclase, and VBD values of ≤ 5.4 wt% that are similar to, or slightly higher than, the range observed in plagioclase (Fig. 9). In accord with Rutherford and Devine (1988), we propose that the amphibole crystals grew deep within the magma system (P > 200 MPa). Taking the entire range of amphibole-hosted glass inclusions in Rutherford and Devine (1988), and applying the model of Moore et al. (1995) at a magma temperature of 900 °C, we calculate a water solubility of 5.8 ± 0.4 wt% at 220 MPa, and 5.5 ± 0.3 wt% at 200 MPa. Once again, the data point to water-saturation of amphibole-bearing magma at pressures of ~ 200 MPa. The pressure at which amphibole began to crystallise is not constrained, as Rutherford et al. (1985) and Rutherford and Devine's (1988) experiments place no upper pressure limit on amphibole stability. However, Merzbacher and Eggler (1984) have shown that amphibole is the sole liquidus phase in water-undersaturated liquids with ≥6 wt% water at a pressure of 400 MPa.

The melt inclusion data suggest that phenocryst growth, as well as microlite growth, may also have occurred under polybaric water-saturated conditions. Moore and Carmichael (1998) and Sisson and Grove (1993) have previously proposed that decompression of water saturated andesite and basalt is responsible for phenocryst growth. To test the possibility that plagioclase phenocryst growth in MSH dacites was largely a response to ascent of water-saturated magma, we have used the experimental data of Rutherford et al. (1985) to calculate the amount of crystallisation that occurs when water-saturated magma undergoes near-isothermal decompression. To do this, we have taken the reported phase assemblages and compositions of experimental run products from their Series 2 (FMO, water-saturated) and Series 5 (NNO, water saturated) experiments and derived phase proportions over a range of P and T using a least squares fitting routine. Rutherford et al. (1985) report compositions of all phases except oxides in some runs. Where Fe–Ti oxide data for a particular runs are not reported we have used data from the experimental starting material (white dacite pumice SH-084). This assumption has little bearing on the results of our calculations, which are presented in Table 2 and Fig. 10a.

Two features of Table 2 and Fig. 10a are remarkable. The first is the very small standard deviations on the modal proportions, testifying to the lack of zoning and good equilibration of the run products in these experiments. The second feature is the dramatic increase in crystallinity, notably of plagioclase, with decreasing pressure. At 215 MPa, 922 °C, QFM the melt is close to its liquidus and amphibole is the only crystalline phase (5 wt%). By 125 MPa, 890 °C, the rock is only 69% melt, with 26% plagioclase crystals (An₅₆) and no amphibole. Overall, the phase proportions under these latter conditions are in good agreement with the mode of the 18 May white dacite (62-66% glass, 25-30% plagioclase, < 10% mafics; Kuntz et al. 1981; Cashman and Taggart 1983; Melson 1983) and with that of grey dacite SH80D (Table 2). Note that 30-40% isothermal crystallisation over this pressure interval is in good agreement with the calculations for the water-saturated Qz–Ab–Or system at 800 °C (Fig. 2b).

A decompression-driven crystallisation model can also explain the phenocryst textures. Plagioclase crystals are euhedral, with well-developed, oscillatory-zoned rims (e.g. Pearce et al. 1987; Cashman 1992). Both of these features are consistent with plagioclase crystallisation during isothermal (or adiabatic) ascent under water-saturated conditions. Corroded plagioclase cores may represent relict material from the source region, or crystals grown at high pressures, which became resorbed during the water-undersaturated phase of magma ascent (cf. Fig. 2c). In contrast, amphibole phenocrysts are commonly strongly embayed and irregular in form (Pearce et al. 1987). This is consistent with the decreasing mode of amphibole at pressures < 215 MPa (Fig. 5a). Note that at pressures < 150 MPa at 920 °C and < 100 MPa at

Table 2 Calculated phase proportions for water-saturated experiments of Rutherford et al. (1985); calculation method described in text. The symbol < denotes phases reported as present but with calculated proportions within 1 SD of zero. Modal proportions of

880 °C (Fig. 5a) amphibole is no longer a stable crystallising phase, and any entrained amphibole phenocryst will form breakdown rims (Rutherford and Hill 1993 and above). The absence of such rims in the white pumice from 18 May 1980 indicates that either decompression crystallisation did not proceed to pressures below amphibole stability or, if it did proceed to such low pressures, it was not stored for more than a few days prior to extraction and eruption. We suggest that phenocryst crystallisation proceeded to pressures of $\sim 150-160$ MPa, and that the slightly lower crystallinity under these conditions, as determined experimentally (Fig. 10a), is partially offset by the presence of several per cent entrained crystals, possibly from the lower crustal source region (Blundy et al. 1999), at the point of water-saturation.

To illustrate that plagioclase crystal resorption is a feature of water-undersaturated magma ascent we have taken the experimental data of Beard and Lofgren (1991) on a andesite bulk composition (57 wt% SiO₂) containing \sim 1.6 wt% H₂O. For experiments at constant temperature (1,000 °C) and pressures of 100, 300 and 690 MPa we have plotted the phase proportions calculated from mass balance (Fig. 10b). Note that during decompression the melt fraction increases because of increasing $a_{\rm H2O}$, in stark contrast to water-saturated decompression. By combining Fig. 10a, b it is possible to see how ascent of a magma with an initial water content that is below saturation leads first to resorption of entrained crystals and then to crystal growth once the saturation pressure is attained.

We contend that at the point of segregation from its source region at pressures $\gg 200$ MPa Mount St Helens dacite magma was water-undersaturated, with $\sim 5-6$ wt% dissolved H₂O and some entrained crystals, predominantly of plagioclase. During the water-undersaturated phase of ascent this plagioclase was partially resorbed. At, or just prior to, water saturation, amphibole, then orthopyroxene, then plagioclase and oxides, saturated as liquidus phases (Figs. 5a and 8). Decompression crystallisation of a water-saturated magma containing plagioclase and amphibole phenocrysts from ~ 200 to ~ 150 MPa can explain the phase

phenocrysts in grey dacite SH80D (Holten et al. 1997) and pyroclastic flow samples (Kuntz et al. 1981) from 18 May 1980 shown for comparison. These data are plotted in Fig. 10a

Run	P	T	f_{O_2}	Glass	Amph	Plag	Opx	Usp	Ilm
141a	240	912	FMQ	98(1)	2(1)	<	< b	_	_
153a	215	922	FMQ	95(1)	5(1)	_	<	_	_
142a	180	916	\overline{FMQ}	84(1)	2.5(6)	12(1)	<	0.8(3)	_
144a	125	890	FMQ	69(2)	< ` `	26(1)	4.3(6)	0.7(3)	0.3(2)
157a	210	922	NNÒ	96(1)	4(1)	< ` ′	< ` ´	- ` ′	_ ` ′
158a	165	923	NNO	83(1)	< ′	14.1(6)	2.8(2)	_	_
$SH80D^{a}$				69	2	24	4	1 ^c	
5/80 ^d				62	3	30	4	1 ^c	_

^a Grey dacite, mode in volume % (Holten et al. 1997)

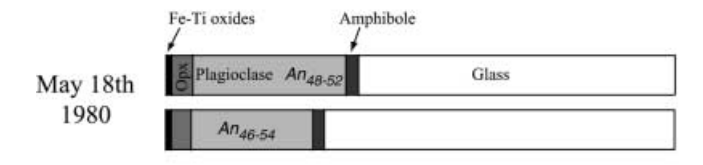
^bPhase present, but proportion within 1 SD of zero

^c1 vol% total oxides (Usp + Ilm)

^dPyroclastic flow sample from Kuntz et al. (1981)

Amphibole

Water-saturated phase relations of MSH dacite at 906-16 °C (Rutherford et al., 1985)



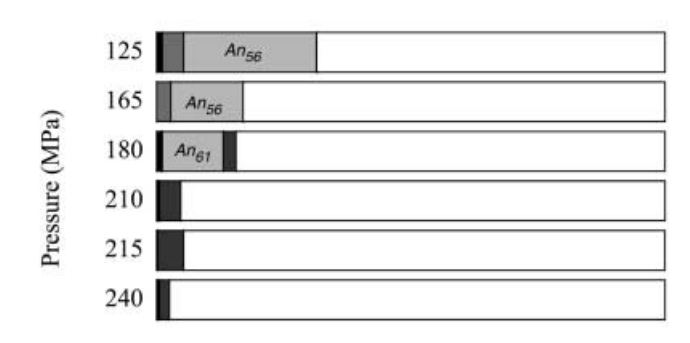
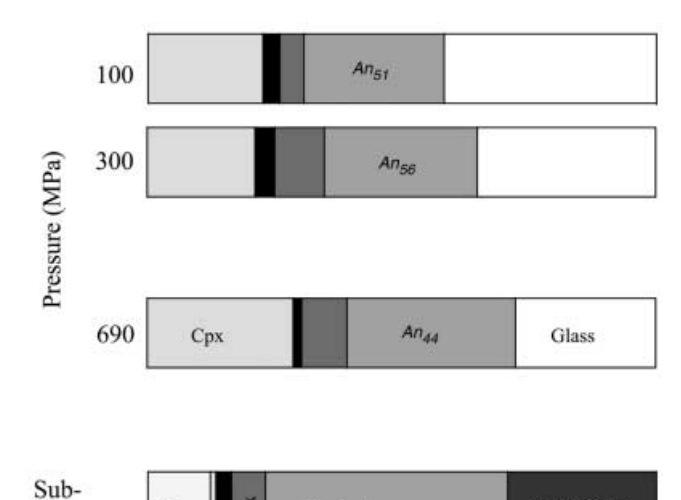


Fig. 10 Phase relations (weight fraction) in hydrous silicic melts at near-constant temperature as a function of pressure under a watersaturated, and **b** water-undersaturated conditions. Phase proportions in a are calculated by least squares mass balance from the data in Rutherford et al. (1985) for experiments equilibrated at 906 ± 16 °C and $f_{\rm O}$, of FMQ or NNO (Table 2). Phase proportions in **b** are from Beard and Lofgren (1991) for andesite (#557) at 1,000 °C. Additionally, in a we present weight fraction mineral modes for a white pumice and a grey pumice from the 18 May 1980 eruption (Table 2), and in **b** show the sub-solidus phase proportions in the andesite starting material. Note in a that crystallinity increases with decreasing pressure, and at a pressure of ~125 MPa the experimental phase assemblage closely matches that of the natural samples, although the experimental plagioclase composition is slightly more calcic and the assemblage lacks amphibole. In **b**, note that crystallinity decreases with decreasing pressure due to crystal resorption

assemblage, the phase proportions, and the phenocryst textures and compositions observed in the 18 May 1980 pumice (Fig. 10a).

Our proposal of a largely polybaric crystallisation history for the Mount St Helens magma differs from that of Rutherford et al. (1985) and Rutherford and Devine (1988), who favour isobaric crystallisation at 220 MPa and water-undersaturated conditions. They base this conclusion not only on the presence of the appropriate phase assemblage in their run products, but also on the appropriate phase compositions: glasses produced experimentally under water-saturated conditions have SiO₂ contents that are lower than those of the white dacite groundmass. Glass SiO₂ content is largely a function of crystallinity, which is higher in water-undersaturated experiments. However, a potential drawback to their experimental approach to constraining pre-eruptive magmatic conditions is that isobaric, equilibrium experiments are used to simulate a natural process that appears to be dominated by decompression

b Water-undersaturated phase relations of andesite at 1000°C (Beard & Lofgren, 1991)



Plagioclase

Fe-Ti oxides

solidus

fractionation. Fractional crystallisation de facto produces more evolved (SiO₂-rich) compositions than equilibrium crystallisation, wherein melt and crystals continuously re-equilibrate. This difference is most marked in the case of plagioclase, which, during decompression fractional crystallisation, will grow by zoning overgrowth. Plagioclase zoning was not significant in the experiments listed in Table 2, all of which are fully equilibrated at the experimental P and T. As a result, although the phase compositions in the waterundersaturated (fluid $X_{H_2O} \approx 0.67$; $f_{O_2} = NNO + 1.5$) experiments of Rutherford et al. (1985) and Rutherford and Devine (1988) match those of the natural samples, the phase proportions do not. Conversely, although proportions in water-saturated experiments match those in the natural samples, phase compositions are consistently slightly less evolved, e.g. melt SiO₂ (anhydrous) of 70 ± 1 wt% versus 73%, melt CaO 3.6 \pm 0.2 wt% versus 2.6%, plagioclase composition of An₅₆ versus An₄₆₋₅₃ (Rutherford et al. 1985). We consider this small mismatch reflects fractional crystallisation in the natural sample (e.g. zoned plagioclase) versus equilibrium crystallisation in the experimental samples (e.g. homogeneous plagioclase). It is also worth noting that the experiments of Rutherford et al. (1985) summarised in Fig. 10a were performed at temperatures 20–30 °C higher than the 895 ± 15 °C proposed by Rutherford and Hill (1993) for the white pumice. This fact will also tend to increase melt SiO₂ and plagioclase An content relative to the natural samples.

Polybaric crystallisation of phenocrysts is also consistent with petrological changes in eruptive products following the 18 May 1980 event. Phenocryst plagioclase increased in abundance (up to 32%), whereas hornblende decreased both absolutely (from 4 to 1.5%) and

relative to orthopyroxene (Cashman and Taggart 1983), and the Fe–Ti oxides recorded decreasing temperatures (Cashman 1992). At the same time, the melt inclusions within plagioclase phenocrysts became more silicic and more water-poor (Melson 1983). These observations suggest that, with time, phenocryst crystallisation (and amphibole breakdown) continued to increasingly shallow levels beneath the volcano. At the same time, the persistence of amphiboles without reaction rims (Rutherford and Hill 1993) suggests that some magma continued to be supplied from deeper levels during this period. Mixing of deeper and shallow magmas, and associated re-heating and remobilisation, seems a plausible explanation for the textural heterogeneity of many dacite samples and their phenocrysts.

Conclusions

Based on compositional variation in natural and experimental glasses from Mount St Helens dacites we have arrived at the following model for magmatic crystallisation at pressures < 300–400 MPa (Fig. 8). Magma ascending from the source region, possibly partially molten hydrous basalt at pressures > 700 MPa (Blundy and Gardner 1997), consists of a silicate melt with < 10% phenocrysts of amphibole, orthopyroxene, clinopyroxene(?) and calcic plagioclase. Some of these phases may represent entrained source material (or 'restite') from depth (Blundy et al. 1999), whereas others may be phenocrysts grown en route to shallow levels. This episode of crystallisation at Mount St Helens will be discussed in greater detail elsewhere. The melt composition at this stage is dacite with ~ 68 wt% SiO₂ (anhydrous), as preserved in melt inclusions in amphibole (Rutherford and Devine 1988). The water content of the melt is ~ 6 wt%; magma temperature is ~ 900 °C.

At a pressure of ~ 300 MPa, i.e. just prior to water saturation (Fig. 8), the magma begins to crystallise amphibole and possibly orthopyroxene. On reaching saturation at pressures of ~200 MPa water exsolves and the melt crystallises plagioclase (An $_{\sim 60}$) and Fe–Ti oxides in addition to amphibole and orthopyroxene. With further ascent, the proportion of amphibole decreases (and early-formed phenocrysts become resorbed), while the proportion of orthopyroxene and plagioclase increases. At the same time, plagioclase An content decreases, and melt SiO₂ increases. This process is essentially adiabatic, with only a few degrees drop in temperature over a \sim 3km ascent. At a pressure of ∼150 MPa, the magma contains 30–35% phenocrysts, dominated by normally zoned euhedral plagioclase, with minor orthopyroxene and partially resorbed amphibole (Fig. 10a). In the course of polybaric crystallisation the water content of the melt dropped from ~ 6 to ~ 4 wt%, as preserved in plagioclase glass inclusions (Fig. 9). The major Plinian episode of the 18 May 1980 eruption tapped magma at this depth (5–6 km) and transported it rapidly to the surface without further re-equilibration. This depth is

equivalent to the shallow low-velocity region at 4.5–6 km identified by Lees (1992), and suggests that the seismically defined reservoir at > 9 km (Scandone and Malone 1985; Barker and Malone 1991; Lees 1992) marks the region from which melt is re-supplied to shallower levels. We propose that phenocrysts grew during transfer from > 9 km to this shallow chamber, which was largely evacuated during the Plinian phase of 18 May 1980.

Subsequent eruptions produced both pumice and dome samples that equilibrated at pressures $\leq 150 \text{ MPa}$ because of their slow ascent through the sub-volcanic plumbing system. It appears that during any one eruption magmas were sampled from a variety of levels within the sub-volcanic system. This is a natural consequence of ascent up a conduit that remains full, or partially full, of magma between eruptions. Slow ascent of these variously hybrid magmas promotes decompression-driven fractional crystallisation, predominantly of plagioclase microlites and phenocryst rims (An_{30–40}; Cashman 1992). In some cases magma ascended sufficiently slowly, and to sufficiently shallow levels, to encounter the quartz/tridymite-feldspar cotectic. Under these conditions, the first silica phase to saturate was quartz, which forms microlites, or occasionally poikilocrysts, which became resorbed during further ascent. When adiabatically ascending magma reached very shallow depths (\sim 500 m; 11 MPa), it saturated with tridymite instead of quartz. When any magma batch was arrested at shallow depth and allowed to cool, cotectic crystallisation of quartz and feldspar drove residual melt compositions towards higher K₂O contents and the Qz-Ab-Or ternary minimum. Fine-grained spherulitic intergrowths of quartz and feldspar were produced by this process. Some pre-18 May 1980 magma also equilibrated at very shallow pressure in the form of a cryptodome, subsequently preserved as blast dacite, and similar grey dacite (Hoblitt and Harmon 1993). The SiO₂ contents of matrix glass in these samples are close to the postulated location of the 0.1-MPa cotectic in Qz-Ab-Or, consistent with magma arrest 500–1200 m below the original volcanic summit during the spring of 1980.

In summary, we view magma crystallisation at Mount St Helens as a polybaric, near-adiabatic process that approximates fractional crystallisation, in that the dominant phenocryst phase (plagioclase) grows by zoning overgrowth. Crystallisation occurs over a 2- to 4km depth range following water saturation. This range will be increased if other volatile phases, such as CO₂, are present causing volatile saturation at greater depths. The rapidity of plagioclase crystallisation under conditions of rapidly decreasing water pressure may in part account for the ubiquity of oscillatory zoning features in the plagioclase phenocrysts (Pearce et al. 1987). Reheating of shallow magmas by hotter deeper magmas may also have played a role in generating the textural diversity in plagioclase. Melt inclusions are trapped in amphibole and plagioclase phenocrysts prior to and subsequent to volatile saturation, respectively. The water content of these inclusions may therefore reflect the range of depths over which crystallisation occurred, possibly moderated by post-entrapment leakage (e.g. Tait 1992), whereas the composition of the glass indicates the extent of crystallisation. Our proposal is consistent with recent studies of phenocryst growth in continental arc andesite and basalt (e.g. Sisson and Grove 1993; Moore and Carmichael 1998; Brophy et al. 1999) in which relatively rapid water-saturated decompression is considered to be the primary driving force. However, our proposal differs from conventional views of Mount St Helens and many other silicic volcanoes, as epitomised by Rutherford et al. (1985) and Rutherford and Devine (1988), in which crystallisation occurs primarily by cooling in a sub-volcanic magma chamber under near-isobaric conditions, often over long time scales.

Acknowledgements This study is the result of 10 years independent research by J.D.B. and K.V.C. Over this period, J.D.B. acknowledges support through research fellowships from NERC and the Royal Society, and K.V.C. acknowledges NSF grants EAR 8803215, 9017364, 9418008 and 9614753. Thanks to the Fulbright Commission for partial support for an 8-month visit by J.D.B. to the University of Oregon, where this work was written. We very much appreciate the informed and encouraging comments of Steve Sparks, Ian Carmichael, Bill Brown, Tom Sisson, Mac Rutherford and Jake Lowenstern, which helped us to improve and hopefully clarify the manuscript.

References

- Barclay J, Rutherford MJ, Carroll MR, Murphy MD, Devine JD, Gardner J, Sparks RSJ (1998) Experimental phase equilibria constraints on pre-eruptive storage conditions of the Soufrière Hills magma. Geophys Res Lett 25:3437–3440
- Barker SE, Malone SD (1991) Magmatic system geometry at Mt. St Helens modeled from the stress field associated with posteruptive earthquakes. J Geophys Res 96:11883–11894
- Beard JS, Lofgren GE (1991) Dehydration melting and watersaturated melting of basaltic and andesitic greenstones and amphibolites at 1, 3, and 6.9 kb. J Petrol 32:365–401
- Blundy JD, Gardner JE (1997) Origin of Mount St Helens dacites by partial melting of underplated Cascades basalts. J Conf Abstr 2(1):16
- Blundy JD, Cashman KV, Chappell BW (1999) Generation, ascent and crystallisation of dacite magma at Mount St Helens, 1980– 1986. EOS Trans Am Geophys Union 80:F1095
- Bowen NL, Tuttle OF (1950) The system NaAlSi₃O₈–KAlSi₃O₈–H₂O. J Geol 58:489–511
- Brophy JG, Whittington CS, Park Y-R (1999) Sector-zoned augite megacrysts in Aleutian high alumina basalts: implications for the conditions of basalt crystallization. Contrib Mineral Petrol 135:277–290
- Brown WL (1993) Fractional crystallization and zoning in igneous feldspars: ideal water-buffered liquid fractionation lines and feldspar zoning paths. Contrib Mineral Petrol 113:115–125
- Cashman KV (1992) Groundmass crystallization of Mount St Helens dacite, 1980–1986: a tool for interpreting shallow magmatic processes. Contrib Mineral Petrol 109:431–449
- Cashman KV, Blundy JD (2000) Degassing and crystallization of ascending andesite and dacite. Philos Trans R Soc Lond A 358:1487–1513
- Cashman KV, Taggart JE (1983) Petrologic monitoring of 1981 and 1982 eruptive products from Mount St Helens. Science 221:1385–1387
- Conrad WK, Nicholls IA, Wall VJ (1988) Water-saturated and undersaturated melting of metaluminous and peraluminous

- crustal compositions at 10 kb: evidence for the origin of silicic magmas in the Taupo Volcanic Zone, New Zealand, and other occurrences. J Petrol 29:765–803
- Criswell CW (1987) Chronology and pyroclastic stratigraphy of the May 18, 1980 eruption of Mount St Helens, Washington. J Geophys Res 92:10237–10266
- Devine JD, Gardner JE, Brack HP, Layne GD, Rutherford MJ (1995) Comparison of analytical methods for estimating H₂O contents of silicic volcanic glasses. Am Mineral 80:319–328
- Ebadi A, Johannes W (1991) Beginning of melting and composition of first melts in the system Qz–Ab–Or–H₂O–CO₂. Contrib Mineral Petrol 106:286–295
- Elkins LT, Grove TL (1990) Ternary feldspar experiments and thermodynamic models. Am Mineral 75:544–559
- Endo ET, Dzurisin D, Swanson DA (1990) Geophysical and observational constraints for ascent rates of dacitic magma at Mount St Helens. In: Ryan MP (ed) Magma transport and storage. Wiley, New York, p 318
- Fenn PM (1977) The nucleation and growth of alkali feldspars from hydrous melts. Can Mineral 15:135–161
- Fyfe WS (1970) Some thoughts on granitic magmas. In: Newall G, Rast N (eds) Mechanisms of igneous intrusion. Geol J Spec Issue 2:201–216
- Gardner JE, Carey S, Rutherford MJ, Sigurdsson H (1995) Petrologic diversity in Mount St Helens dacites during the last 4,000 years: implications for magma mixing. Contrib Mineral Petrol 119:224–238
- Geschwind C-H, Rutherford MJ (1992) Cummingtonite and the evolution of the Mount St Helens (Washington) magma system: an experimental study. Geology 20:1011–1014
- Geschwind C-H, Rutherford MJ (1995) Crystallization of microlites during magma ascent: the fluid mechanics of 1980–1986 eruptions at Mount St Helens. Bull Volcanol 57:356–370
- Hammer JE, Cashman KV, Hoblitt R, Newman S (1999) Degassing and microlite crystallization during the pre-climactic events of the 1991 eruption of the Mt. Pinatubo, Philippines. Bull Volcanol 60:355–380
- Hildreth W (1981) Gradients in silicic magma chambers: Implications for lithospheric magmatism. J Geophys Res 86:10153– 10192
- Hoblitt RP, Harmon RS (1993) Bimodal density distribution of cryptodome dacite from the 1980 eruption of Mount St Helens, Washington. Bull Volcanol 55:421–437
- Holten T, Jamtveit B, Meakin P, Cortini M, Blundy J, Austrheim H (1997) Statistical characteristics and origin of oscillatory zoning in crystals. Am Mineral 82:596–606
- Holtz F, Pichavant M, Barbey P, Johannes W (1992a) Effects of H₂O on the liquidus phase relations in the haplogranitic system at 2 and 5 kbar. Am Mineral 77:1223–1241
- Holtz F, Johannes W, Pichavant M (1992b) Effect of excess aluminum on phase relations in the system Qz–Ab–Or. Experimental investigations at 2 kbar and reduced H₂O-activity. Eur J Mineral 4:137–152
- James RS, Hamilton DL (1969) Phase relations in the system NaAlSi₃O₈–KAlSi₃O₈–CaAlSi₂O₈–SiO₂ at 1 kilobar water vapour pressure. Contrib Mineral Petrol 21:111–141
- Johannes W (1980) Metastable melting in the granite system Qz–Ab–Or–An–H₂O. Contrib Mineral Petrol 72:73–80
- Johannes W, Holtz F (1996) Petrogenesis and experimental petrology of granitic rocks. Springer, Berlin Heidelberg New York
- Klug C, Cashman KV (1994) Vesiculation of May 18, 1980 Mount St Helens magma. Geology 22:468–472
- Kuntz MA, Rowley PD, MacLeod NS, Reynolds RL, McBroome LA, Kaplan AM, Lidke DJ (1981) Petrography and particlesize distribution of pyroclastic-flow, ash-cloud, and surge deposits. US Geol Soc Prof Pap 1250:525–540
- Lees JM (1992) The magma system of Mount St Helens: non-linear high-resolution P-wave tomography. J Volcanol Geotherm Res 53:103–116
- Lipman PW, Mullineaux DR (1981) The 1980 eruption of Mount St Helens, Washington. US Geol Surv Prof Pap 1250

- Lipman PW, Norton DR, Taggart JE Jr, Brandt EL, Engleman EE (1981) Compositional variations in 1980 magmatic deposits. In: Lipman PW, Mullineaux DR (eds) The 1980 eruption of Mount St Helens, Washington. US Geol Surv Prof Pap 1250, pp 631–640
- Luth WC, Jahns RH, Tuttle OF (1964) The granite system at pressures of 4 to 10 kilobars. J Geophys Res 69:759–773
- Melson WG (1983) Monitoring the 1980–1982 eruptions of Mount St Helens: compositions and abundance of glass. Science 221:1387–1391
- Merzbacher C, Eggler DH (1984) A magmatic geohygrometer : application to Mount St Helens. Geology 12:587–590
- Moore G, Carmichael ISE (1998) The hydrous phase equilibria (to 3 kbar) of an andesite and basaltic andesite from western Mexico: constraints on water content and conditions of phenocryst growth. Contrib Mineral Petrol 130:304–319
- Moore G, Vennemann T, Carmichael ISE (1995) Solubility of water in magmas to 2 kbar. Geology 23:1099–1102
- Morse SA (1970) Alkali feldspars with water at 5 kbar pressure. J Petrol 11:221–253
- Pallister JS, Hoblitt RP, Crandell DR, Mullineaux DR (1992) Mount St Helens a decade after the 1980 eruptions: magmatic models, chemical cycles, and a revised hazards assessment. Bull Volcanol 54:126–146
- Pearce TH, Russell JK, Wolfson I (1987) Laser interference and Nomarski interference imaging of zoning profiles in plagioclase phenocrysts from the May 18, 1980 eruption of Mount St Helens, WA. Am Mineral 72:1131–1143
- Rutherford MD, Devine JD (1988) The May 18, 1980 eruption of Mount St Helens. 3. Stability and chemistry of amphibole in the magma chamber. J Geophys Res 93:11949–11959
- Rutherford MJ, Devine JD (1996). Pre-eruption pressure-temperature conditions and volatiles in the 1991 dacitic magma of Mount Pinatubo. In: Newhall C, Punongbayan R (eds) Fire and mud: eruptions and lahars of Mount Pinatubo, Philippines. University of Washington Press, Seattle, pp 751–766
- Rutherford MJ, Hill PM (1993) Magma ascent rates from amphibole breakdown: an experimental study applied to the 1980–1986 Mount St Helens eruption. J Geophys Res 98:19667–19686
- Rutherford MD, Sigurdsson H, Carey S, Davis A (1985) The May 18, 1980 eruption of Mount St Helens. 1. Melt composition and experimental phase equilibria. J Geophys Res 90:2929– 2947
- Scandone R, Malone SD (1985) Magma supply, magma discharge and readjustment of the feeding system of Mount St Helens during 1980. J Volcanol Geotherm Res 23:239–262

- Schairer JF (1950) The alkali feldspar join in the system NaAlSiO₄– KAlSiO₄–SiO₂. J Geol 58:512–517
- Scheidegger KF, Federman AN, Tallman AM (1982) Compositional heterogeneity of tephras from the 1980 eruptions of Mount St Helens. J Geophys Res 87:10861–10881
- Sisson TW, Grove TL (1993) Temperatures and H₂O contents of low-MgO high alumina basalts. Contrib Mineral Petrol 113:167–184
- Swanson DA, Dzurisin DRTH, Iwatsubo EY, Chadwick WW, Casadevall TJ, Ewert JW, Heliker CC (1987) Growth of the lava dome at Mount St Helens, Washington, 1981–1983. Geol Soc Am Spec Pap 212:1–16
- Symonds RB, Reed MH (1993) Calculation of mutlicomponent chemical equilibria in gas-solid-liquid systems: calculation methods, thermochemical data, and applications to studies of high-temperature volcanic gases with examples from Mount St Helens. Am J Sci 293:758–864
- Tait SR (1992) Selective preservation of melt inclusions in igneous phenocrysts. Am Mineral 77:146–155
- Tuttle OF, Bowen NL (1958) Origin of granite in the light of experimental studies in the system NaAlSi₃O₈–KAlSi₃O₈–SiO₂–H₂O. Geol Soc Am Mem 74
- Whitney JA (1988) The origin of granite: the role and source of water in the evolution of granitic magmas. Geol Soc Am Bull 100:1886–1897
- Williams DL, Abrams G, Finn C, Dzurisin D, Johnson DJ, Denlinger R (1987) Evidence from gravity data for an intrusive complex beneath Mount St Helens. J Geophys Res 92:10207– 10222
- Winkler HGF, Ghose NC (1973) Further data on the eutectics in the system Qz–Or–An–H₂O. N Jahrb Mineral Monatsh, pp 481–484
- Winkler HGF, Boese M, Marcopoulos T (1975) Low temperature granitic melts. N Jahrb Mineral Monatsh, pp 245–268
- Winkler HGF, Das BK, Bretibart R (1977) Further data of lowtemperature melts existing on the quartz + plagioclase + liquid + vapour isobaric cotectic surface within the system Qz-Ab-Or-An-H₂O. N Jahrb Mineral Monatsh, pp 241-247
- Wolf KJ, Eichelberger JC (1997) Syneruptive mixing, degassing and crystallization at Redoubt Volcano, eruption of December 1989 to May, 1990. J Volcanol Geotherm Res 75:19–37
- Yoder HS (1968) Albite–anorthite–quartz–water at 5 kbar. Carnegie Inst Wash Yearbook 66:477–478
- Yoder HS, Stewart DB, Smith JR (1957) Ternary feldspars. Carnegie Inst Wash Yearbook 56:206–214